MONTE CARLO MODELING OF THE GAMMA KNIFE PERFEXION™

BY

RYAN C.M. BEST

A Thesis Submitted to the Graduate Faculty of

WAKE FOREST UNIVERSITY GRADUATE SCHOOL OF ARTS AND SCIENCES

in Partial Fulfillment of the Requirements

for the Degree of

MASTER OF SCIENCES

in the Department of Physics

December 2010

Winston-Salem, North Carolina

Approved By:

J. Daniel Bourland, Ph.D., Advisor

George Holzwarth, Ph.D.

Freddie R. Salsbury Jr., Ph.D.

TABLE OF CONTENTS

LIST OF TABLES AND FIGURES

LIST OF ABBREVIATIONS

Model 4C	GK model preceding Perfexion
Model B	Early (1997) model of GK
Co-60	Cobalt-60
CT	Computed Tomography
FWHM	Full width at half-max
GK	Gamma Knife
GSR	Gamma stereotactic radiosurgery
LGP	Leskell GammaPlan
LINAC	Linear Accelerator
MC	Monte Carlo
MeV	Mega electron-volts
MR	Magnetic resonance
OF	Output factor
OSLD	Optically stimulated luminescence dosimeters
PE	Photoelectric Effect
PENELOPE	PENetration and Energy LOss of Positrons and Electrons in matter
PSF	Phase space file
SRS	Stereotactic radiosurgery
TLD	Thermoluminescent detector
Model U	Early (1987) model of GK
high-Z	high atomic number

ABSTRACT

Best, Ryan C.M.

MONTE CARLO MODELING OF THE GAMMA KNIFE PERFEXION™

Thesis under the direction of
J. Daniel Bourland, Ph.D., Associate Professor of Radiation Oncology,
Biomedical Engineering, and Physics (Adjunct)

The Gamma Knife Perfexion™ is a radiosurgical treatment device used to irradiate targets in the head such as tumors, blood vessel defects, and malfunctioning nerves. It uses 192 high activity Cobalt-60 sources collimated to a common focus to impart radiological damage to the target structure while minimizing dose to adjacent healthy tissue a few millimeters away. Tungsten collimators are organized into eight sectors of 24 sources each, and can independently choose one of three collimation sizes for each sector. The largest collimator size is designed to produce a sphere of dose 16 mm in diameter at the focus. The smaller collimators produce dose spheres 8 mm and 4 mm in diameter. Planning for Gamma Knife stereotactic radiosurgery (GK SRS) is performed using images from computed tomography (CT) and/or magnetic resonance (MR) imaging, as well as manual skull measurements. The software used to plan the delivery of these treatments uses a simplistic set of assumptions that do not consider heterogeneous tissue structures (e.g., bone, air) and instead assume everything under the skin surface is radiologically equivalent to water. This assumption enables rapid calculations for water-equivalent tissues; however, it also leads to errors in the calculation of radiation dose near heterogeneities.

Monte Carlo (MC) methods that model radiation interactions and track radiation transport have been demonstrated to calculate dose more accurately in heterogeneous volumes than

other dosimetry models. MC methods use random sampling of precalculated probability distributions to determine the paths each particle of ionizing radiation takes one step at a time, recording the energy imparted at each step along each path. The large computation time required for MC calculations has historically limited its use for daily dose computation; however, the MC approach can be a very powerful tool for research purposes.

This study used Penelope, an established set of Monte Carlo codes, for modeling to better understand the geometric and radiological physical characteristics of the Elekta GK Perfexion, as relevant for GK SRS accuracy, precision, and radiation safety. Specifically, this work 1) implements a MC computation model for GK dose calculations; 2) models the Elekta GK Perfexion irradiation geometry within a MC program; and 3) determines using MC computation the relative dose rate factors, known as output factors (OF), for the three collimator sizes (16 mm, 8 mm, 4 mm), relative to the 16 mm collimator. Both individual row OFs and average collimator OFs have been determined, as required for the Perfexion geometry. The collimator OFs are compared both to experiment and to Monte Carlo based simulations performed by manufacturer, Elekta AB. The row OFs cannot be measured experimentally, and are therefore compared only to the Monte Carlo-based results provided by the manufacturer.

INTRODUCTION

Small field dosimetry

Radiation dosimetry is the measurement of energy imparted per unit mass by ionizing radiation to matter.[1] External beam radiation therapy uses one or more beams of ionizing radiation that are aimed from outside the patient and shaped to closely conform to the shape of a target volume, such as a tumor. Medical physicists have long used a standard 10x10 cm^2 field as the reference field for dosimetry calculations since that size is about the average field size for early radiotherapy treatments. For dose rate calibrations a linear accelerator (LINAC) beam is collimated to form a square 10 cm on a side and a radiation dosimeter, typically an ion chamber, is placed on the beam's central axis at a prescribed depth in a material at a reference distance from the source. In clinical use the goal is to cover an entire tumor with a comfortable safety margin of about 1 cm. This margin is included due to uncertainty in definition of the target volume as well as to account for patient motion. As radiation oncology and medical physics have progressed smaller, more conformal fields are being used that irradiate target tissues with close margins while minimizing exposure to adjacent healthy tissue. There is no consensus definition of a "small field", but Das reports that a field size of less than 3x3 cm^2 "needs special attention in dose measurements and in dose calculations."[2] From a physics point of view, a small field is one where lateral electronic equilibrium is compromised and not obtained, or field flatness is compromised, as shown in figure 1. Essentially, the field size is smaller than the average range of the secondary electrons and electronic equilibrium, whereby the charged particles leaving the dosimetric region of interest are compensated for by others that enter the volume, is not obtained.[3] Dose measurements under non-equilibrium conditions are very challenging.

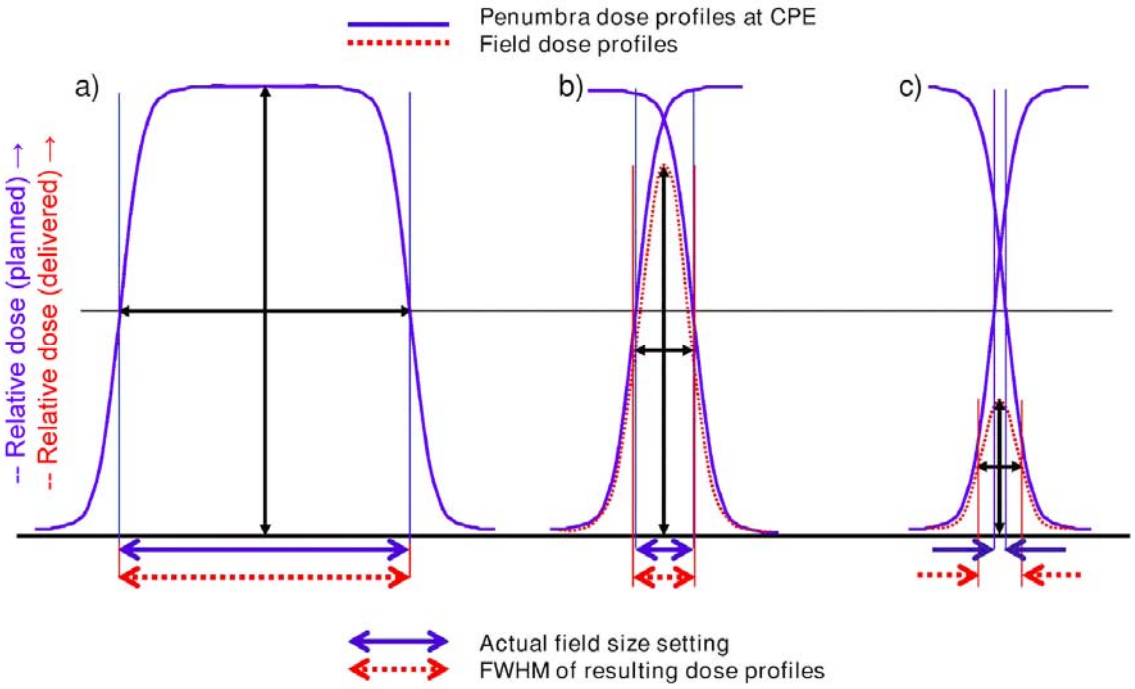

Figure 1: The penumbra is caused by the finite size of the source, and radiological scatter from collimating components and the interaction material (water equivalent phantom). For large square fields (a), the penumbra is a relatively small proportion of the dose compared to the central plateau, where the y-axis is relative dose. For small fields (b,c), the entire beam can be within the penumbra.[2] The figure shows how full width at half max (FWHM) becomes a progressively less accurate description of field size as field size shrinks.

The study of small field dosimetry is important for gamma stereotactic radiosurgery (GSR) since the largest field sizes used in GSR are 16 mm or 18 mm in diameter, falling below the common threshold size stated by Das. The 3x3 cm^2 rule also assumes the use of a 10x10 cm^2 single beam.[4,5] A GSR device cannot produce a beam of that size, nor can it have only one source active. Thus, the standard dosimetry procedure does not apply to the small beams used in GSR because 1) small field dosimetry measurements are challenging because of finite detector sizes and 2) only small fields are possible and it is not possible to use a 10x10 cm^2 reference field. Monte Carlo (MC) dose computation is a promising alternative option when dosimetry measurements are difficult to obtain.[2] There

are three primary difficulties associated with small field size dosimetry: penumbra, lateral electron range, and detector size.

Dosimetry for uniquely-sized fields is typically scaled according to measurements from known, measured field data. For small fields, the size of the source of radiation becomes far more important as the proportion of the field within the edge penumbra, the less-than-full-strength irradiation at the beam fringes, increases, as seen in figure 1. MC simulations may assume a point source of radiation, or, as relevant for small fields, may simulate a finite-sized source to ensure accurate modeling of penumbra.

Lateral electron range and charged particle equilibrium are also significant to small field dosimetry. When high-energy photons produce ionizations, most of the charged particles generated proceed in a forward direction relative to the photons, but some electrons travel laterally (e.g. the photoelectrons and Compton electrons). At the beam edges, the laterally traveling electrons enter areas unirradiated by the primary photon beam fluence. Lateral electron range is highly energy dependent,[6] so a zero-field size beam's penumbra size depends on the beam energy and essentially represents a dose kernel for an infinitesimal beam. The Klein-Nishina cross section, shown in figure 2, describes the photon scattering angle as a function of the incident photon energy. The energy dependence is less significant for nearly monoenergetic Cobalt-60 (γ_1 = 1.17 MeV, γ_2 = 1.33 MeV), but photon energy losses after scattering off the collimator walls will cause small spectral changes. Compton interactions are the dominant effect for photons above 100 keV in our simulations.[7] As shown in figure 2 the odds of lateral scattering increase as particle energy drops.

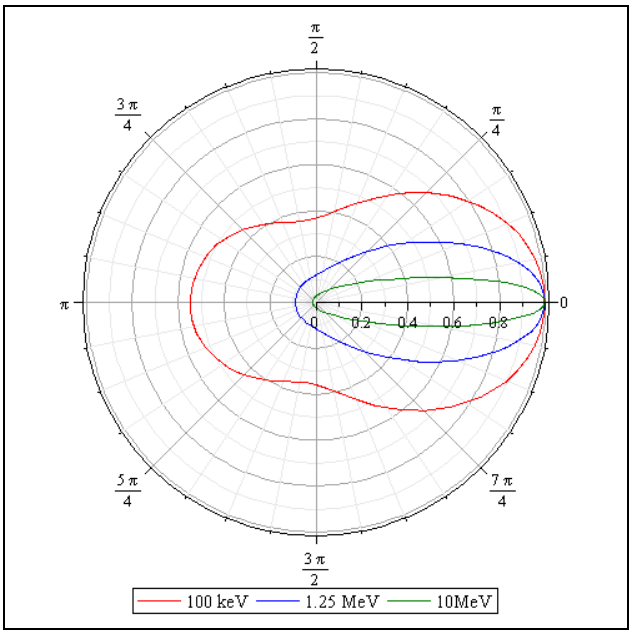

Figure 2: The Klein-Nishina cross section describes the scattering of charged particles and photons after Compton interactions. Particles are incident from the left and interact at the center of the plot. The isocurves show the relative probability of photon scattering through given angles. For any angle, an isocurve's distance from the edge of the plot indicates the probability of scattering through that angle. Colors indicate how incident energy changes the probability of scattering through each angle. Forward bias increases with energy.
(Image by the author based on an equation in Salvat[8])

In addition to the two photopeaks for Cobalt-60, a photon spectrum will also show Compton edges generated by the maximum energy a photon can impart on a free electron.[7] Equation 1 shows the source of Compton edges, where hv is the photon energy and mc^2 is the rest energy of the electron (0.511 MeV). T_{max} is the peak kinetic energy that can be imparted to an electron.

$$T_{\max} = \frac{2hv}{2 + mc^2 / hv} \tag{1}$$

Given the photopeak energies of Cobalt-60, we expect to see Compton edges at 1.12 MeV and 0.960 MeV. These peak energy interactions occur in a direct hit, a 180-degree photon deflection, according to figure 2.

The photoelectric effect (PE) dominates photon interactions at low energies, below 100 keV.[7] Under this effect, photons are absorbed by bound electrons, which leave their shell with energy equal to the photon's kinetic energy minus their binding energy.

The MC system used in this work, Penelope[8] by Salvat et al., uses K-shell cross sections calculated by Sauter[9] to simulate energy depositions and angular deflections under photoelectric interactions.[8] The Sauter distribution is shown in figure 3.

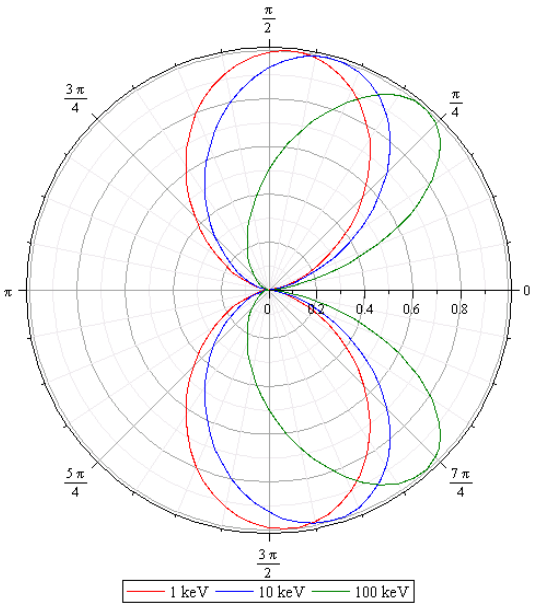

Figure 3: The Sauter distribution describes the angular deflections of photoelectrons. Since PE photons always scatter laterally, they are responsible for much of the dose deposited outside the central photon beam. Photons with higher initial energy tend to cause more forward-directed scattering. (Image by the author based on an equation in Salvat[8])

Pair-production interactions occur when a photon passes close to an atomic nucleus, creating an electron-positron pair. Twice the electron rest energy, 0.511 MeV, is required for this interaction to occur, so only the 1.33 MeV Cobalt-60 gamma has enough energy for pair-production. If pair-production is taking place, a recorded spectrum should show a

peak at the difference between the initial photon energy and twice the electron rest energy. In this case the difference is approximately 308 keV.[7]

Small field dosimetry is also difficult due to the finite size of dosimeters, and the fact that any dosimeter necessarily perturbs the field it measures. The simplest measurement device is an ion chamber, which relies on Bragg-Gray cavity theory, stating that the chamber is only nonperturbing if the range of charged particles is greater than the diameter of the chamber cavity. For a sufficiently small chamber, maintenance of electronic equilibrium[10] across the chamber volume becomes prohibitive, however, dose measurements can be made based on the Bragg-Gray principle. Small detectors, such as small and micro ion chambers, diamond detectors, and thermoluminescent detectors (TLDs) are useful for measuring dose at the central plateau of the beam, the beam's output factor[11,12], but cannot provide accurate data off-center due to dose gradient, which prevents charged particle equilibrium and averaging over peaks and valleys of signal. In the future, even these micro-detectors will be too large to provide useful data with smaller photon beams.

A Monte Carlo approach provides a much-needed alternative to experiment. Existing work has validated the MC approach to high energy photon dosimetry.[13,14,15] MC essentially allows a detector size of zero, eliminating spatial effects on dose, and eliminating the perturbing effects of dose measurement. Dosimetry characteristics can be found by measuring a plane of data, then using a scaling factor measured experimentally (at a peak, flat-dose area for example) or by direct calculation of dose. These dose distributions are calculable even when electronic equilibrium is absent,[16] an advantage over measurement.

History of Monte Carlo simulations in radiation transport

MC methods first appeared in physics literature in an article by Kahn[17] in 1950 and the topic's publication rate has increased steadily since that time.[18] Monte Carlo simulations use random number generators to pick among a series of probability distributions to simulate step-by-step the path of an ionizing radiation particle through a given geometry, recording dose deposited along the way. The earliest simulations were conducted by hand in a lab book. Later, enormous mainframes took months to calculate thousands of particle histories. Now, 10^8 histories can be simulated in simple geometry on a standard laptop computer in under an hour.

A simple example of a Monte Carlo simulation is the calculation of step length, *s*, within a homogenous media.[19] In equation 2, λ is the mean free path for the particle given its energy and the attenuation coefficient of the medium, and ζ is a random number from zero to one.

$$s = -\lambda \ln(1-\zeta) \tag{2}$$

A series of ζ will produce a set of distances *s* that match the exponential attenuation of radiation found in experiment. Given that radiation is emitted isotropically from a point source, it is easy to demonstrate how random numbers can be used to choose the initial direction of travel for a particle, choose its initial energy from a given spectrum, and pick what type of interaction occurs based on more probability distributions. Once the interaction occurs, deposited energy is recorded and the new direction of travel calculated, the process begins again with the less-energetic secondary particle.

This type of thorough, microscopic simulation is extremely accurate but computationally expensive, especially for the simulation of electrons. The slowing down of an electron in aluminum from 0.5 MeV to 1 keV takes around 10^4 collisions.[20] A comparably energetic photon takes only a few hundred collisions to come to a stop. This difference is shown in figure 4, where the photons show few turning points and the electrons bend their paths frequently. Most modern Monte Carlo simulations now use a condensed history or macroscopic approach for certain types of computationally-intensive interactions in order to keep simulation times reasonable.

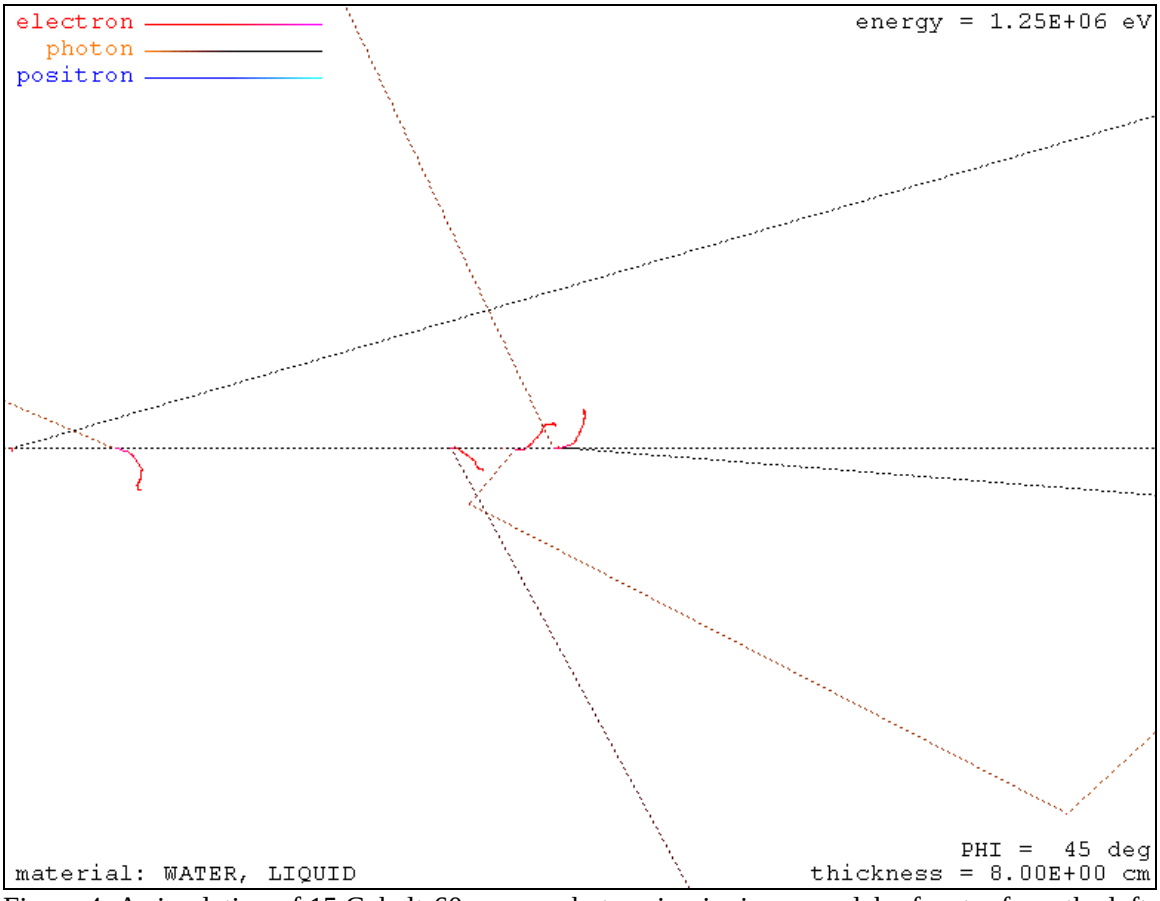

Figure 4: A simulation of 15 Cobalt-60 energy photons impinging on a slab of water from the left. The orange/black photons travel in long, straight paths before their few interactions. (Black photons are higher energy than orange photons.) The few red electrons generated by photon interactions follow short, tortuous paths. Note that the length of the red electron track is roughly proportional to the angle of deflection by the ionizing photon. (Image by the author)

Penelope background and theory

Penelope is a Class II or mixed procedure[21] Monte Carlo simulation system which divides electron and positron collision events into “soft” and “hard” events. Photons are simulated in a detailed way, event-by-event, without approximations. In the energy ranges of concern for this experiment the positron contribution will be negligible. Hard electron events are distinguished by a significant change in the electron’s direction or a significant deposition of charge, characteristics which are positively correlated. Soft events deposit less energy and result in smaller changes in direction. Soft events are approximated and not simulated in a detailed way. The energy thresholds for distinguishing between hard and soft events are configurable in Penelope, so the degree of approximation is adjustable at the cost of longer computing time.[8] The default Penelope energy thresholds of 10 keV for electron simulation were used in this work. For high energy electrons, the differential cross sections (DCS) for interactions drop off quickly for larger scattering angles and increased energy loss.[22] Thus, relatively few interactions will take place on that track and each individual event can be simulated for little computational cost. Even in large numbers, soft events have little effect on the particle’s direction. Soft events therefore use a multiple scattering approach, where low energy events are dropped along a straight track at fixed intervals without individual computation.

Penelope in practice

Penelope is experimentally verified in the literature, demonstrating its effectiveness at accurately predicting the behavior of ionizing radiation. Papers typically compare Penelope to other Monte Carlo implementations as well as to experiment.[8,22-29]

Sempau et al. modeled an electron beam from a LINAC head using Penelope as well as BEAM and DOSEXYZ, codes based on another MC modeling package called EGS4.[24] Modeling a LINAC is in many ways more difficult than modeling a device with a radioactive source like Cobalt-60. Radiations from radioactive sources have well-defined energies (monoenergetic photons and continuous electron energies), but the exact energies and spectrum of a LINAC can vary from machine to machine, and can be tuned. Sempau modeled the complex internal geometry of a Siemens Mevatron LINAC using the Penelope geometry engine, PENGEOM.

PENGEOM uses simple geometric shapes described in quadric geometry to define the area to be modeled. Planes, cylinders, cones, paraboloids, and other shapes are defined and pieced together into homogeneous bodies. Many bodies pieced together can form complex shapes, like the head of a LINAC or simplified patient anatomy.[8]

Quadric surfaces are defined by the reduced quadric equation, eq 3. Plotting where $F_s=0$ shows a surface whose shape is defined by the I_n coefficients, which can each be set to -1, 0, or 1. Setting I_n=(1,1,1,0,-1) produces a sphere, I_n=(1,1,0,0,-1) produces a cylinder about the z-axis, I_n=(1,1,-1,0,0) produces a cone, and so on. Paraboloids, hyperboloids, and planes can also be created.

$$F_s(x,y,z) = I_1x^2 + I_2y^2 + I_3z^2 + I_4z + I_5 \quad (3)$$

PENGEOM defines a volume from a surface by a side pointer which is set to ±1 per surface, indicating which direction is “filled”. A side pointer of -1 on a spherical surface produces a solid ball of material, while a side pointer of +1 would fill everything outside the sphere. A second, planar surface could divide the ball into a hemisphere, and which side remains is determined by the plane’s side pointer. Scaling factors are used to turn spheres into ellipsoids, or turn cones narrower or wider, etc. This robust quadric geometry is used by Penelope due to its low computational cost compared to voxelized geometries.[8]

Penelope includes a useful tool for separating this type of problem into several steps: A phase space file (PSF) of particles can be recorded at a certain plane in one step of the simulation, then the PSF can be played back exactly at the next step. For Sempau’s simulation a plane was defined at the exit window of the accelerator so every particle leaving the complex geometry of collimators, flattening filter, etc. was recorded into the PSF. For the next step, the previously simulated complex geometry of the LINAC was retained in the PSF, and to save computer time the PSF was played back as a beam of particles impinging on a slab of water. Two types of detectors were used to measure the output in the water and both were compared with the Penelope and BEAM results along the central axis, and several lateral planes. For the 6 MeV beam, Penelope was consistent with experiment, with no more than 3% error in depth dose and 5% error in lateral dose. For the 18 MeV beam, Penelope’s depth dose results were within 3.5% and lateral dose results were within 5.5%. Lateral dose errors are larger in part due to the difficulties in accurately measuring the position and dose experimentally at the beam edges, where a penumbra of dose exists. Between BEAM and Penelope, small but significant differences

were found in their PSFs. These variations were attributed to differences in the way the two algorithms simulate physics. The differences were “not very significant” in the calculation of final dose distributions.[24]

The Leskell GammaPlan (LGP) dosimetry software which is used to plan GK treatments has shortcomings which are discussed later in detail. LGP assumes all material is either air or water, which causes predictable problems when the beams interact with bone and air cavities deep to the skin surface. LGP does not use image data for dose computation, so the dose calculation model is unaware of the presence of any materials other than those that are water equivalent. MC is generally well-suited for the heterogeneous material problem, and Penelope in particular due to its high accuracy at interfaces between materials[30] and high-Z materials.[31] Several studies discussed below compared MC results to LGP predicted results.

Penelope was used by Moskvin et al. to model the Gamma Knife model 4C.[25] PENGEOM was used to design the internal collimating structures of a single source (the 4C has 201 sources) and a PSF was collected at the exit of the secondary collimator. The single source was modeled at five planes at fixed distances down the beam path in air. The results were compared to experiments using film dosimetry. Using previously-published information about source locations[32], Moskvin modeled the collected PSF as originating from each of the 201 source origins. The output of each PSF was recorded on a dose plane within a simulated plastic 16 cm diameter homogeneous dosimetry sphere. Film was placed inside an identical experimental sphere and was compared to the calculated dose distribution plane. The dose distribution plane was also calculated in LGP.

Comparison of the 50% isodose curve diameters in Penelope, film, and LGP found small discrepancies but overall strong agreement. The general shapes of the isodose curves were followed closely in each simulation method, with the largest differences at 0.5 mm, and less than 0.2 mm, which is within Elekta specifications in either case. The strong agreement between LGP and Monte Carlo methods in this case was due to the homogenous nature of the dosimetry sphere.

When the same team later used the same Penelope-generated GK PSFs on a heterogeneous sphere the results were different. They built a dosimetry sphere with air cavities and simulated bone to more accurately model the human head, then modeled an identical head phantom in PENGEOM.[28] Dosimetry differences in this case were as much as 7% near air/tissue interfaces due to secondary electron disequilibrium and lowered energy deposition near the heterogeneous areas. The authors proposed the inelegant solution of simply plugging all the sources whose beams passed through air cavities. It is surprising that LGP still uses a very simple algorithm for dose calculation (exponential attenuation: $e^{-\mu x}$) when linear accelerator treatment planning software packages like Pinnacle and Eclipse have used CT data to estimate attenuation characteristics of pixel-sized regions for many years. Elekta AB is working on both convolution and MC models that will require a CT image for dose computation, with higher-fidelity results expected for heterogeneous media

METHODS AND MATERIALS

Gamma Knife Perfexion

The Elekta Gamma Knife (GK) Perfexion is a GSR treatment device that collimates gamma ray radiation from 192 linear sources of Cobalt-60 to a small sphere (4, 8, or 16 mm in diameter) centered about a geometric focus in order to deliver a high radiation dose to a small target positioned at the focus while delivering very little dose to healthy tissue within a few millimeters of the target. The sources are arranged in five rows outside a 30 cm radius tungsten cylinder (nominally 30 cm outer radius, 20 cm inner radius, 10 cm wall thickness) that has precision machined holes to collimate each source to 4, 8, or 16 mm in diameter at a focal point in the center of the device, (figures 5 and 6).[33] Nominal source-to-focus distance is 40 cm, however, as is discussed later, each source row has a unique distance value. Sources are arranged in 8 moveable sectors of 24 sources each. Each sector can move independently to one of four longitudinal positions: fully blocked, 4 mm, 8 mm, or 16 mm positions. In this manner a target located at the focus can be irradiated with a desired grouping of the 8 sectors.

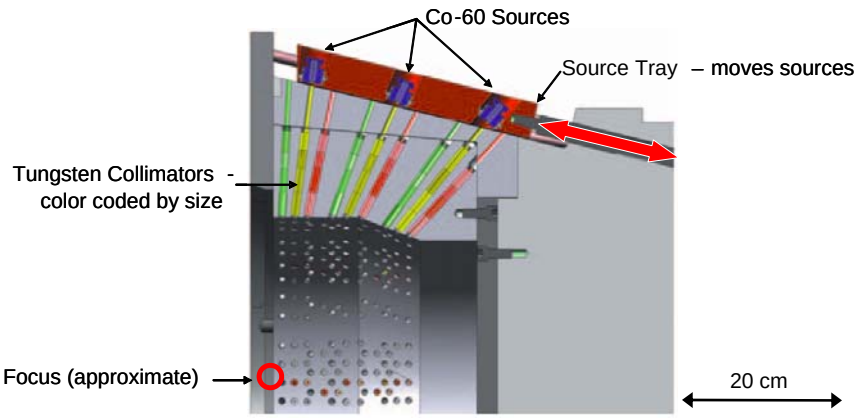

Figure 5: The source arrangement and collimator assembly shown in cross section.[34] Cobalt-60 sources are blue and move together on the source tray in red. Three collimator sizes are shown: 4 mm in yellow, 8 mm in green, and 16 mm in red. Sources move to a collimator to irradiate the focus.

A significant portion of the work involved in MC modeling of the Perfexion is determining and describing the internal geometry of the device accurately. For this reason the details of the GK design will be described at some length.

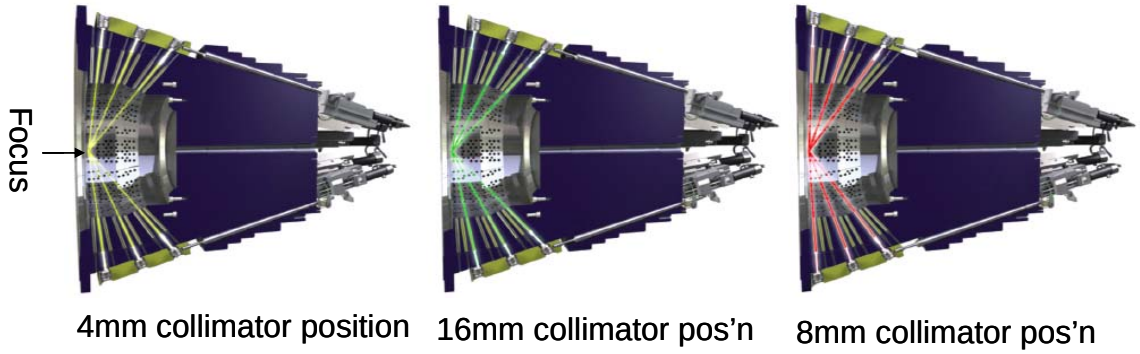

Figure 6: The source tray moves longitudinally to position the sources in the three treatment positions aligned with the three sets of collimators.[33] The figure with yellow beams is the 4 mm collimator, 16 mm in green, and 8 mm in red. The collimators have a common focus. The collimator selected determines the volume irradiated at the focus.

Previous versions of the Gamma Knife underwent few significant changes since the first Model U version (US version, 1987), essentially the original GK device, with 201

sources arranged in a hemispheric geometry at the same distance (40 cm) from the focus. In the Model B (US version, 1997)[34], the 201 static sources were arranged in a vertically oriented hemisphere, again with each source the same distance from the focus as for the Model U (40 cm). The modeling of a nearly spherically-symmetric system was comparatively easy once the geometric coordinates of the sources were known.[32] In contrast, for the Perfexion each sector of 24 sources can be moved independently and the source-to-focus distance is different for each of the five rows of sources within a sector, varying from 37 to 43 cm.[33] In a film taken 8 cm from the isocenter, figure 7 shows the arrangement of the source beams from one sector at the 16 mm setting. Some of the beams in figure 7 are starting to overlap on their way to convergence at isocenter. The row E beams are more ellipsoidal than the row A beams because row E intersected the film at a more oblique angle than row A, which was nearly perpendicular to the film.

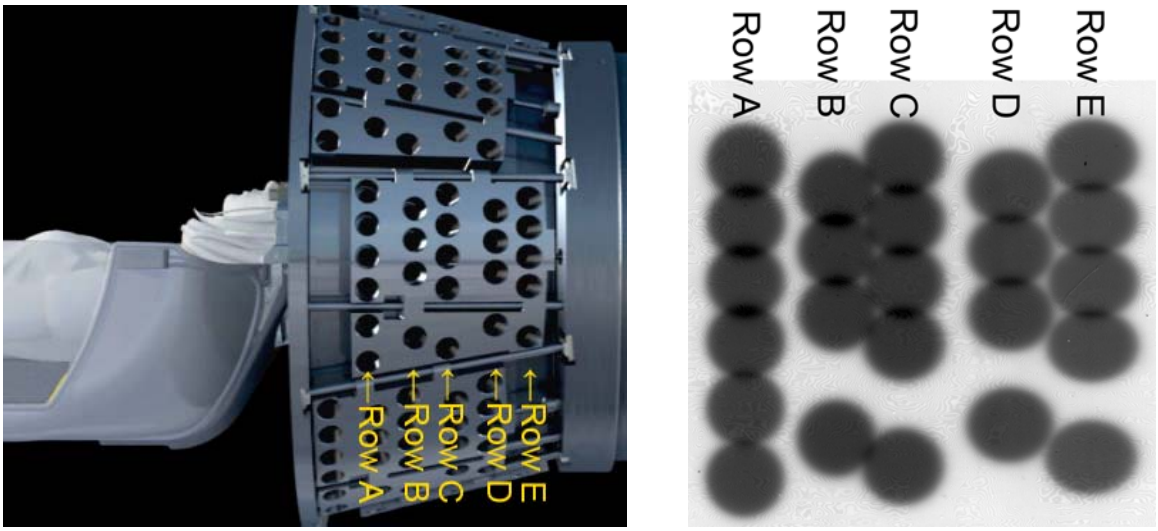

(A) **(B)**

Figure 7: (A) Positioning of sources within a sector. Sectors are visibly in several different collimator positions in this image since the rows are not lined up between sectors. (Image source: Elekta AB)

(B) A radiochromic film taken 8 cm from the isocenter showing the arrangement of Cobalt-60 beams delivered by one sector of the Perfexion. (Image by the author)

In the GK models before Perfexion the 201 sources were fixed in location regardless of the collimator size used – to change the beam size one collimator was dismounted and another manually mounted in its place. With Perfexion's moving source trays, the positions of the sources vary for each collimator size (figure 6). One important aspect of the sources that does not vary between collimator positions is the angular orientation of each linear source within the tray. When the sources are in the 4 mm collimator position, the linear source in its bushing is aligned with the collimator along a common axis. The 4 mm collimator is the only collimator size with this well-aligned geometry. For the 16 mm and 8 mm positions, the source axes are not perfectly aligned with each collimator axis. The angular difference is small, but is significant in a device which demonstrates sub-millimeter dosimetric accuracy.[34] This issue is discussed in more detail later and the small angular difference in alignment is shown in figure 10.

Another unique aspect of the Perfexion relative to the previous models is the ability to use multiple collimation sizes at once. Previous GK models used a collimation helmet that attached prior to treatment. The collimation helmets for the GK Models U, B, and 4C came in four collimator sizes (4, 8, 14, and 18 mm), and it was not possible to mix the collimators of different sizes. The only dose shaping option was to block individual sources entirely, called plugging. Plugging is a time-consuming process performed one source at a time. In the Perfexion, since the eight sectors (24 sources per sector) can be in one of four positions: fully blocked, 4 mm, 8 mm, or 16 mm, unique dose distributions can be produced from a single shot based on clinical needs. See figure 8.

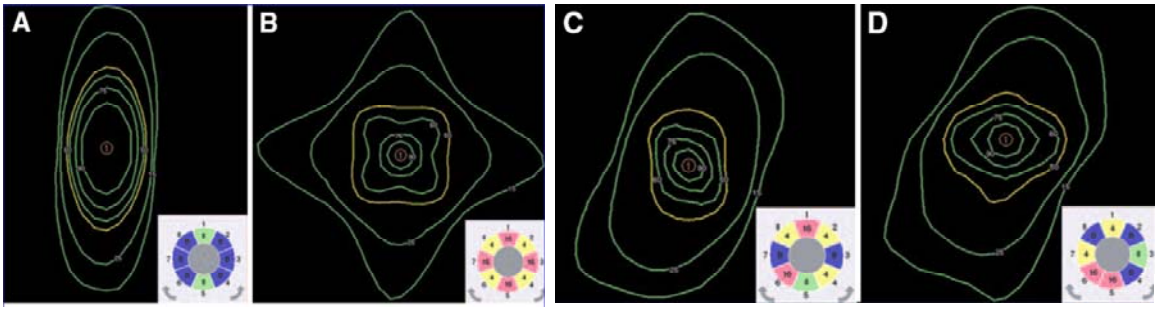

Figure 8: The eight sectors of sources can be sized individually as shown by the small graphics in the bottom right of each figure. When all sectors are collimated the same, the isodose curves in the X-Y plane (constant Z) shown appear roughly circular. The unique shapes seen here are produced by different dose contributions from different directions due to different collimators active in each sector. Shown isodose lines are 15%, 25%, 50% (yellow), 60%, 75%, 90%. (Image by Lundquist et al.[34])

LGP, the proprietary treatment planning software package, handles patient images and uses a simple dosimetry algorithm, exponential attenuation ($e^{-\mu x}$), relative to the dose rate at the focus for an 80 mm radius water-equivalent sphere, to calculate dose within the patient's head as a function of radiological depth for each of the 192 sources. The dose

computation algorithm back-calculates along each source trajectory from the center of a 80 mm radius sphere, using the path length (depth) for each individual shot. Skull radii measurements are used to provide a simple model of the surface of the head, to determine the distance from each source to the skin surface for purposes of dose computation. As stated previously, the LGP algorithm assumes that tissue located under the skin surface is radiologically water equivalent. Several papers have found significant problems with the LGP dose calculation method, especially in heterogeneous regions like bone and air cavities.[28,29] These differences in dose computations may be significant for research conditions such as small animal irradiations which include small, complex anatomical regions.[35]

The most accurate dose computation algorithms use MC calculations that take into account the many radiological parameters of materials present in the irradiated region. A system that accurately simulates physical phenomena will necessarily be more accurate than the simpler approximations currently used. To date, no complete MC simulation of the GK Perfexion exists in the literature.

Output Factors

The output factor for the GK Perfexion model is the experimentally determined dose rate delivered by a specified collimator size, or collimator row, relative to the dose rate delivered by a reference collimator or reference row.[36] Relative to a dose profile curve, which looks similar to a Gaussian distribution, the output is measured across the flat dose plateau (peak dose) at the central region of the dose profile. A collimator output factor is the dose profile curve's height in the plateau region relative to the height of the 16 mm

collimator's profile curve. Since there are five rows and three collimator sizes, fifteen row OFs exist. The fifteen curves for the fifteen row OFs are plotted and the 16 mm-Row B curve's peak region is normalized to unity. Rows of sources cannot be activated individually with the Perfexion, only full sectors of sources consisting of five rows, so row OFs are not measurable on the Perfexion. Only the collimator OFs are measurable experimentally. Elekta provides the row output factors based on their in-house MC calculations, and publishes these numbers with each patient treatment plan and online.[37] The collimator output factors are also provided by Elekta, again based on their own MC simulations and small detector measurements.

Collimator output factors, in MC simulations, are the weighted sum of the row outputs normalized to the 16 mm collimator output. The weighting factor, W, is the number of sources in the given row: 6 sources in row A, 4 in row B, and so on up to the 24 sources in a sector as seen in figure 7 and equation 4. Weighting is required because the row OFs assume only one source per row.

$$OF_{coll} = \frac{\sum_{i=A,B,C,D,E} W_i \cdot OF_{Row-i}}{24} \tag{4}$$

$$W_i = 6,4,5,4,5$$

See table I for the output factors provided by Elekta.

Collimator (mm)	Sources per row	Row	Row OF	Collimator OF
4	6	A	0.799	
4	4	B	0.815	
4	5	C	0.792	0.805
4	4	D	0.725	
4	5	E	0.663	
8	6	A	0.957	
8	4	B	0.946	
8	5	C	0.901	0.924
8	4	D	0.808	
8	5	E	0.730	
16	6	A	0.961	
16	4	B	1.000*	
16	5	C	0.986	1.000*
16	4	D	0.920	
16	5	E	0.851	

TABLE I: Monte Carlo calculated output factors for three collimator sizes and five rows as calculated by Elekta Instrument AB, Stockholm, Sweden.[38] Only the Collimator OFs may be determined experimentally because the rows cannot be activated individually.
(* All row OFs are defined as a fraction of the 16 mm-Row B output. Collimator OFs are relative to the 16 mm collimator output.)

Output factors measurements have been reported in a prodigious number of articles over the several versions of the Gamma Knife, covering dozens of devices capable of measuring ionizing radiation.

- Bednarz et al found the OFs for the GK model U using diamond detectors and miniature ion chambers.[39]
- The OFs of the GK model B were measured by Mack et al., Tsai et al., and Araki et al. using a liquid ion chamber, pin-point ion chamber, diode detectors, diamond detectors, TLDs in microcube and microrod forms, alanine pellets, radiochromic films, silicon

diodes, radiographic film, radiophotoluminescent glass rod dosimeters, and p-type silicon detectors.[40-42]

- Further GK model B OFs were measured using film which also documented the effect of collimator size on end effect times – the time during which the patient is moving into place.[43]
- Measurements on the model 4C Gamma Knife, the version immediately preceding the Perfexion, were performed by Kurjewicz et al.[44] among others using film, optically stimulated luminescence dosimeters (OSLDs)[45], and polymer gels[46].
- GK Perfexion output factor measurements have been performed by Novotny et al. [38] and others[47,48] using various types of film and found their OFs "in good agreement with the vendor recommended Monte Carlo calculated values."

Monte Carlo simulations were used to measure the collimator output factors of previous GK versions with results close to Elekta recommended values.[25,36,49]

Monte Carlo simulation parameters for the GK Perfexion

Source and Collimator Geometry

The bulk of the work on this project consists of accurately modeling the interior geometry of the GK collimators and sources. Initially, significant progress was made mocking up GK geometry based on back-calculating the positions of sources by using radiochromic film images obtained along the beam paths (e.g., Figure 7B). With a non-disclosure agreement with Elekta, simplified machinist plans[50] were made available, allowing a more accurate physical MC simulation. These specifications to a large degree verified our

earlier film-based measurements, locating the source angles no more than one degree off of the radiochromic film-based calculations.

The simplified machinist drawings provided by Elekta describe a slab of tungsten, and concentric cylinders of various diameters forming a collimator straight through this slab. (See figure 9) The distances from the focal point to shielding interfaces and the source bushing are shown. Not shown, but included as data are the collimator angles from normal, and the axial rotation for each source's collimator. These various parameters are confidential information and cannot be stated in this document.

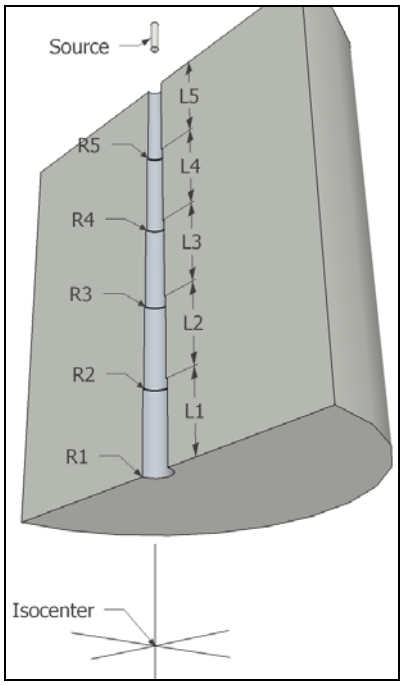

Figure 9: Cutaway of collimator geometry data received from Elekta. Diameters of the collimator at several key points were provided, along with distances to sources and source orientations. The collimator is a series of concentric cylinders drilled out of tungsten shielding. Drawing is not to scale.

The Penelope version 2003 quadric geometry[8] is ideally suited to modeling a simple system of stacked cylinders set on a tilt. More complex to model using quadric geometry

were the individual GK sources and source bushings which are made up of six nested cylinders.[51]

Not shown in figure 9 are the small tilts and shifts of the source bushing, which vary for each collimator row and collimator size. Since the sources move along a fixed channel to each of the collimating positions, the source's central axis can only be coaxial with one source position, which is the 4 mm collimation position. For the 16 mm and 8 mm collimators the source axes sit at a small angle relative to the collimator axes, as shown in figure 10.[50] Precise values vary for each collimator row. These small angular changes in the source-collimator alignment have an effect on output factors since the effective width of a linear source increases when it sits at an angle instead of end-on.

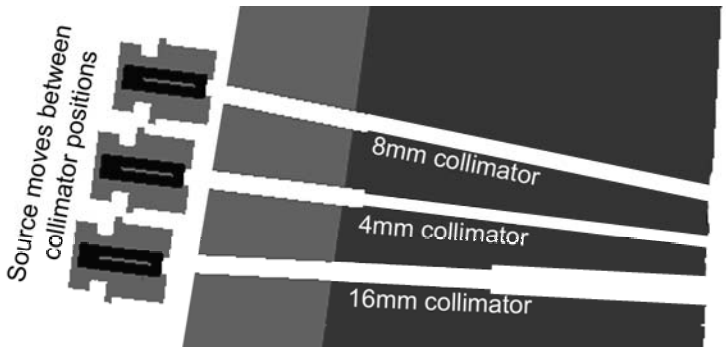

Figure 10: A single Cobalt-60 source can move between three collimator positions. In the 4 mm position the source and its bushing are aligned with the collimator. In the 16 mm and 8 mm positions the source and bushing are not on a common axis with the respective collimators, and are slightly oblique.

Accurate modeling of the source shape is also important. An initial model assumed a point source centered in the source bushing. Elekta's sealed source registration drawings[51] show the source is just under 2 cm in length, which at a distance of 38 cm to the isocenter seems like a small difference. Output factors calculated under the point

source assumption were off by around 10% from the manufacturer's published values. By defining three point sources along the central axis of the modeled source the output factor errors were reduced to under 5%. The current model uses seventeen point sources set about 1 mm apart along the 17 mm length of the cobalt source, as seen in figure 11. Seventeen was selected because the cylinder of Cobalt is nominally 17 mm long and 1 mm in diameter.

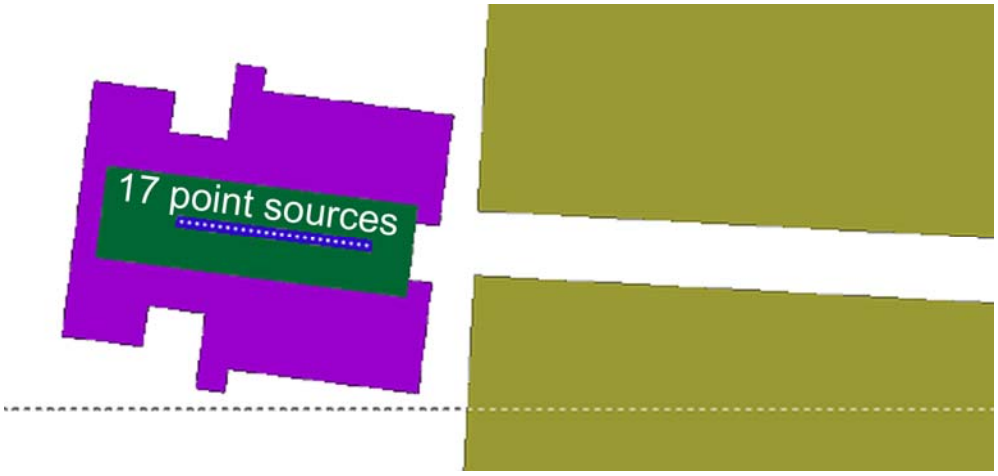

Figure 11: The simulation modeled seventeen point sources of radiation (white dots in the middle of the bushing) along the Cobalt volume inside the source bushing.

The 2008 version of Penelope allows definition of linear sources which should eliminate problem of approximating a linear source as discrete points by randomly selecting a source position along a line for each individual photon shower.[52]

Photon fluence definition

Although an isotropic source fluence would be more physically realistic, it would require about 90 times more initial photons to achieve similar statistical certainty in the final OF results. In our internal tests we found a 3-degree cone, measured from the center line to the beam edge, was sufficient. The closest GK source row is approximately 38.5 cm from

isocenter, so an uncollimated 3-degree cone would be 4 cm across at isocenter. The extra width provides authentic scattering effects within the collimator.

Initial photon energy was randomly selected from the two energies (γ_1 = 1.17 MeV, γ_2 = 1.33 MeV) that Cobalt-60 emits, with each energy emitted 50% of the time. Each of the seventeen points emitting photons along the linear source emitted $2.35*10^4$ initial photons, for a total of about $4*10^5$ initial photons per GK source. This number of initial photons is lower than the number used by other simulations of earlier GK models,[25,28] but we were able to make up for the difference by making use of phase space files, discussed in detail below, to achieve similar levels of statistical significance in output factor results. Internal testing against larger phase space files showed smaller files could be played back repeatedly with no difference in dosimetric results, and only modest cost in terms of statistical significance.

Dose calculation grids and volumes

The theoretical dosimeter consisted of a sphere of air 3.3 mm in diameter simulated at the center of the sphere. A three-dimensional 1.5 cm grid of dose was recorded over the center of the dosimetry sphere. The grid was 100x100x100, producing a bin size of 0.15 mm cubes. The dose deposited in the 3.3 mm diameter region of interest was collected from the grid using a Matlab program. These dose grids were also used to produce dose profile curves.

Methods to improve efficiency and reduce variance

Three principal methods were used to improve simulation efficiency and reduce variance in dosimetric results: 2-step simulation via phase-space files, particle splitting, and interaction forcing.

1. Phase Space Files- 2 step simulations: Monte Carlo simulations of linear accelerators and other radiosurgical devices are typically divided into multiple steps.[24] First, particles are generated at a small- or point-source within a given energy spectrum and directed toward the target within a cone, limiting the initial directions. After interacting with various shielding and beam-modifying components, but before reaching the patient or target volumes, the particles hit a limiting plane which records their final state (position, direction, and energy) into a phase space file (PSF). After recording the PSF, the second step of the simulation is simply playing-back the PSF particles. There are several ways dividing the simulation in pieces improves efficiency.

Of the initially-generated particles, sometimes only a small fraction reaches this recording plane. For some 4 mm collimator simulations, less than 1% of the initial photons reach the PSF plane and are recorded. Since the PSF is typically played back several times, the PSF eliminates the need to simulate particles which will never make it near the target. Additionally, it eliminates the need to simultaneously model the entire geometry to be simulated. Dividing the process into steps allows first a collimator to be modeled, then on playback the collimator is removed and the target volume put in place. Minimizing the complexity of geometry to be modeled significantly improves simulation speed. A final advantage of multi-step simulations using PSFs is the target geometry needs not be defined during the first step. Once recorded, the PSF can be played back to

impart fluence on a phantom, simulated animal anatomy, voxelized patient anatomy, or any other target.

MC modeling is the ideal method for investigating these subtle differences since it is possible to determine the dosimetric differences across a single beam, including energy differences within a beam, by analyzing the PSF. Experimental methods such as film or gel dosimetry cannot record such spectral information.

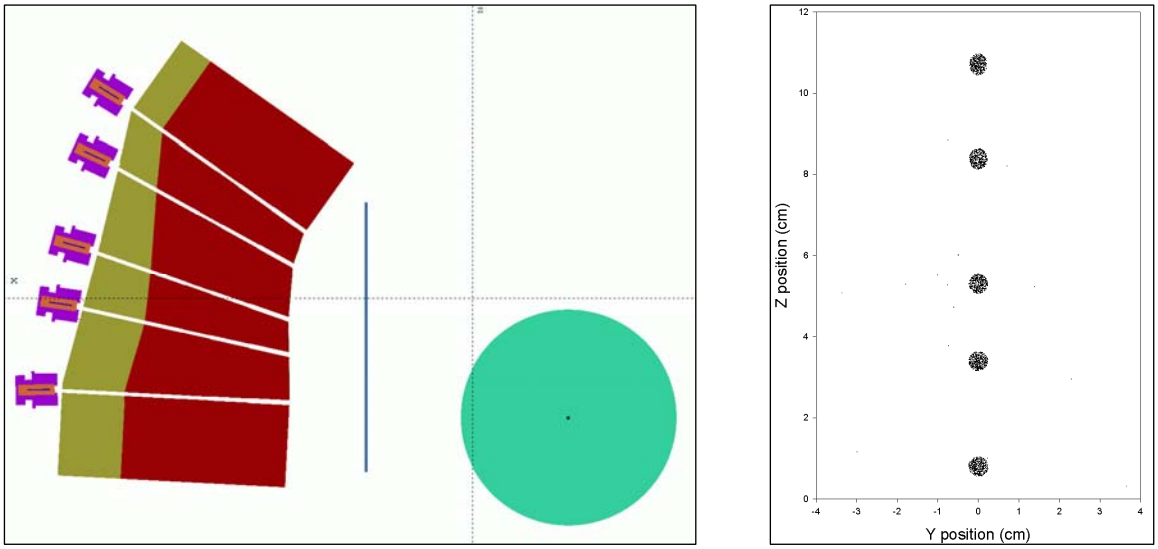

Figure 12: On the left in the cross-section of a simulation geometry, the plane where a phase space file was recorded is visible as a vertical plane between the collimated channels and the target dosimetry sphere. On the right is a selection from a recorded PSF. Groups of dots indicate where photons hit the plane. Note the groups go from circular to elliptical as the angle of incidence goes from near-normal to oblique.

Simulations generated photons at the position of the Cobalt-60 source and directed them within a 3-degree cone, measured from the beam center, down the series of concentric cylinders that make up a GK collimator. Photons which passed out of the tungsten collimator assembly reached the PSF plane, shown in figure 12, and were recorded. Photons reaching this plane were mostly near their initial energies of 1.33 or 1.17 MeV,

although a predictable amount of the spectrum was also filled with lower energy scattered photons. On playback, the photons are sequentially re-emitted from their recorded position in the recorded direction with the recorded energy toward the target of choice.

2. Interaction forcing: Every dose deposition recorded in a Monte Carlo simulation includes an uncertainty. The simplest way to reduce uncertainty is to increase the number of particles depositing dose. When increasing the number of histories alone is not enough, forcing interactions becomes useful. Interaction forcing is a technique that increases the odds a particle passing through a certain area will interact while reducing by an equal weight the dose deposited in such an interaction.[8] For a given small volume of interest far from the particle source, the odds of any particle reaching the volume may be very low, and the small probability the particle will react in that volume reduces the odds further. Statistical error applied to doses in forced volumes is reduced by artificially increasing the number of interactions in those volumes.

Interaction forcing works by reducing the mean free path of a particle by the specified weight, w. Several tricks correct for the induced distortions this artificially-increased interaction probability produces. First, deposited energy D applied by forced interactions in the volume are reduced to D/w. Secondary particles generated in weighted interactions have their weights reduced to $1/w$ as well. Third, the state variables of the forced interaction particles are changed only with a probability of $1/w$. Meaning, the energy and direction of movement are changed only if a random number is less than $1/w$ arises.

The Penelope input file allows the user to apply an interaction-forcing number to a simulated body for each particle type, and for each type of interaction. In our simulation the volume of interest is a 3.3 mm diameter sphere of air inside a larger sphere of Acrylic,

representing a small-volume ionization chamber inside a spherical phantom. Our facility uses a Capintec PR-05P Mini-Chamber for annual dose constancy measurements in the Perfexion. This cylindrical ion chamber has a diameter of 6.4 mm, which is larger than our simulated measurement volume.[53] Given the relatively small volume and low density of the target, initial dose uncertainties were sometimes larger than the calculated dose. After applying interaction forcing the uncertainties were reduced to less than 5%.
For simulations reporting output factor results, forcing factors of 100,000 were applied to the volume of air used in OF calculation. Since dry air is approximately 1,000 times denser than water,[7] and mass attenuation coefficients for air and water are similar in the simulated energy range, this forcing factor makes interactions in the air volume of interest approximately 100 times more likely than interactions in an identical volume of water. Forcing allows convergence toward output factor results with fewer total photon showers simulated.

3. Particle Splitting: Particle splitting is the repeated simulation of a single initial particle with the statistical weight of each cloned particle reduced by the inverse of the number of particles.[8] Splitting is typically applied to small regions of a simulation where more particle histories are needed to reduce variance in that region. Splitting was used on the initial particles played back from the phase space file. With a splitting number S, each particle in the PSF is initiated S times with an initial weight w of $1/S$. Since the random numbers applied to the first interaction after initiation are unlikely to ever repeat, particles with identical beginnings travel down different paths almost immediately. Beyond trivially-small simulation sizes, particle splitting leaves the simulation unbiased.[54] Splitting numbers up to 10,000 were used when simulating phase space files.

Since $4*10^5$ initial photons were simulated per GK source, the effective number of initial particles simulated exceeded 10^9 in some cases when the splitting number and phase space file are taken into account. Given that this is preliminary research, this number of simulations is likely in excess of what is necessary to achieve convergence on a statistically significant answer in most cases, depending on what aspect of the simulation is under investigation.

Collimator output factor calculation and dependencies

Output factors are calculated by measuring the dose deposited to a small volume of air at the center of the dosimetry sphere. We measured dose to a spherical volume 3.3 mm in diameter. The dose deposited in this volume, reported in electron volts, was recorded for each row's output. The absolute value of the dose is not critical outside of spectroscopy measurements, so only doses relative to the reference collimator outputs are reported here. Ideally an output factor is the dose deposited at the infinitesimal point of maximum dose, but any useful measurement must take place over a finite volume. We measured the output factor over a range of volumes ±1.6 mm diameter centered on the volume of the 3.3 mm diameter sphere.

Computational Resources

All Monte Carlo-based radiation simulations are examples of embarrassingly parallel problems, a class of problems where pieces of the problem can be computed in parallel without the need for communication between the parallel tasks.

Computations were performed on Wake Forest's DEAC Linux cluster, a centrally-managed high-performance computing environment consisting of 140 computer nodes capable of performing about 1300 simultaneous-jobs.[55]

In this work between ten and fifty computers were given identical portions of the simulation at a time and the results summed or merged. Our code provided each simulation instance with a different set of pseudorandom seeds generated by the Linux command $RANDOM in a Bash shell. Penelope internally generates its own random numbers thereafter. At peak computation times, 150 jobs were performed simultaneously over approximately 20 hours per simulation. Under typical circumstances, depending on geometry, a node computed 700-3000 showers per second, where a shower is complete simulation of a primary particle and all secondaries.

RESULTS

Energy Spectra

A simple check on the validity of the simulation is found in the photon energy spectrum delivered to the dosimetry sphere, shown in figure 13. This energy spectrum matches the expected results for radioactive decay of Cobalt-60. This result indicates that both photon generation and subsequent interactions are being modeled properly.

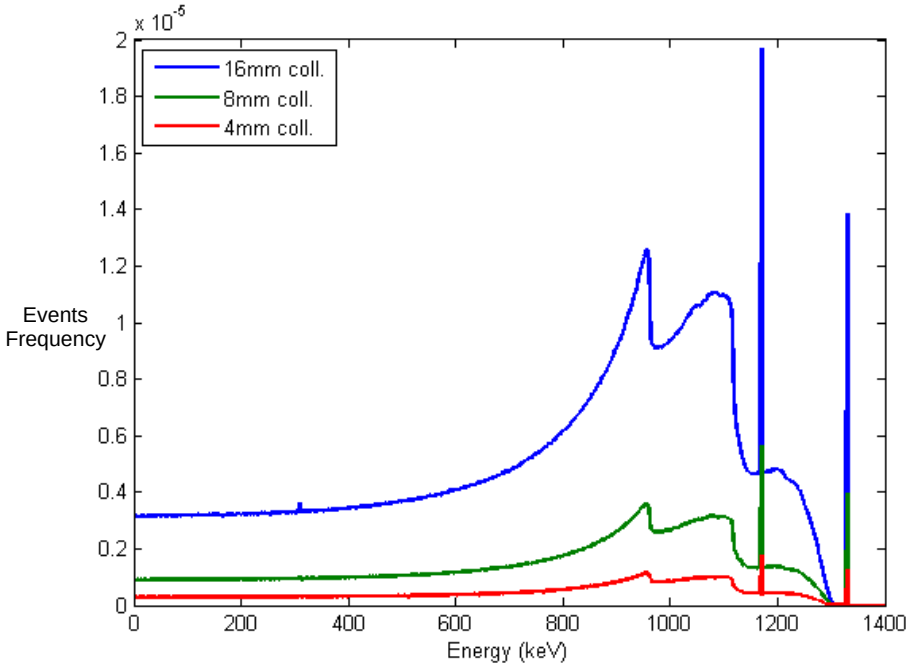

Figure 13: Photon spectra delivered to the dosimetry sphere. The two energy peaks for Cobalt-60 (γ_1 = 1.17 MeV, γ_2 = 1.33 MeV) are clearly visible, along with other scattering phenomenae.

The two Cobalt-60 photopeaks are clearly visible. Compton edges are also visible at 1.12 MeV and 0.960 MeV, as predicted by equation 1, along with decaying probability of interaction to the left of the edges, as predicted by the Klein-Nishina cross section from figure 2.

Also very slightly visible in figure 13 is a peak at 308 keV caused by pair-production interactions induced by the 1.33 MeV gammas. The peak appears at the energy difference between the peak photon energy and twice the rest mass of the electron, the energy MeV Cobalt-60 gammas because they lack enough energy to produce two charged particles,[7] which require 1.22 MeV.

Spectra from all three collimators are shown in figure 13 to illustrate that collimator size had an effect only on the magnitude of the spectra, not the energies detected. When the three plots are normalized they overlap too closely to be differentiable.

Three-dimensional dose distributions

As an initial qualitative check on the geometry of this MC code, a 3x3x3 cm dose grid was recorded at the center of the 8 cm radius dosimetry sphere for each row of each collimator. Central planes from the dose grids are shown in figure 14, showing that each row is at least roughly aimed properly. A tiny sphere of air modeled in the center can be seen by the perturbation of the dose distribution “downstream” of the bubble. Since the particles traveling through the air lose less energy than adjacent particles traveling through the dosimetry sphere material, the particles traversing the air region arrive at the far side of the bubble with more energy to deposit, visible as a red streak in the middle of the yellow beam.

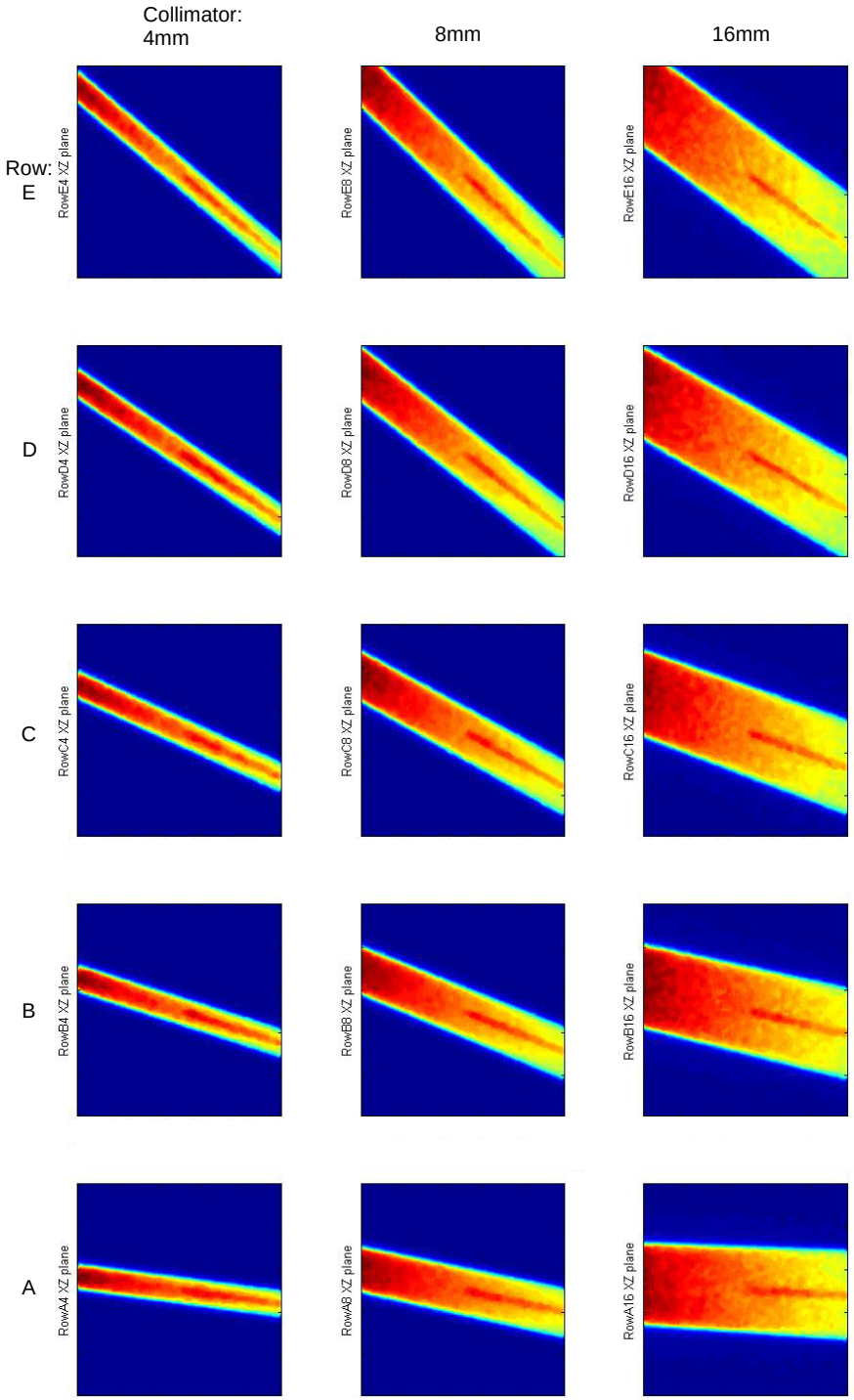

Figure 14: 3x3 cm dose distribution planes from each collimator and source with 1 mm diameter sphere of air at the isocenter. The data from each plane shown here could be used to calculate a row output factor. This dose distribution method has one source per row and was used to calculate row output factors. For all dose distribution images: Red areas are high dose, blue is low dose, on a linear scale normalized independently for each sub-image. (e.g.: Dark red dose regions for Row B16 are not the same absolute dose level as dark red dose regions for Row E4.)

Figure 15 shows the data from each row summed for each collimator over a smaller 2x2x2 cm dose grid, further demonstrating the collimated beams are intersecting as expected.

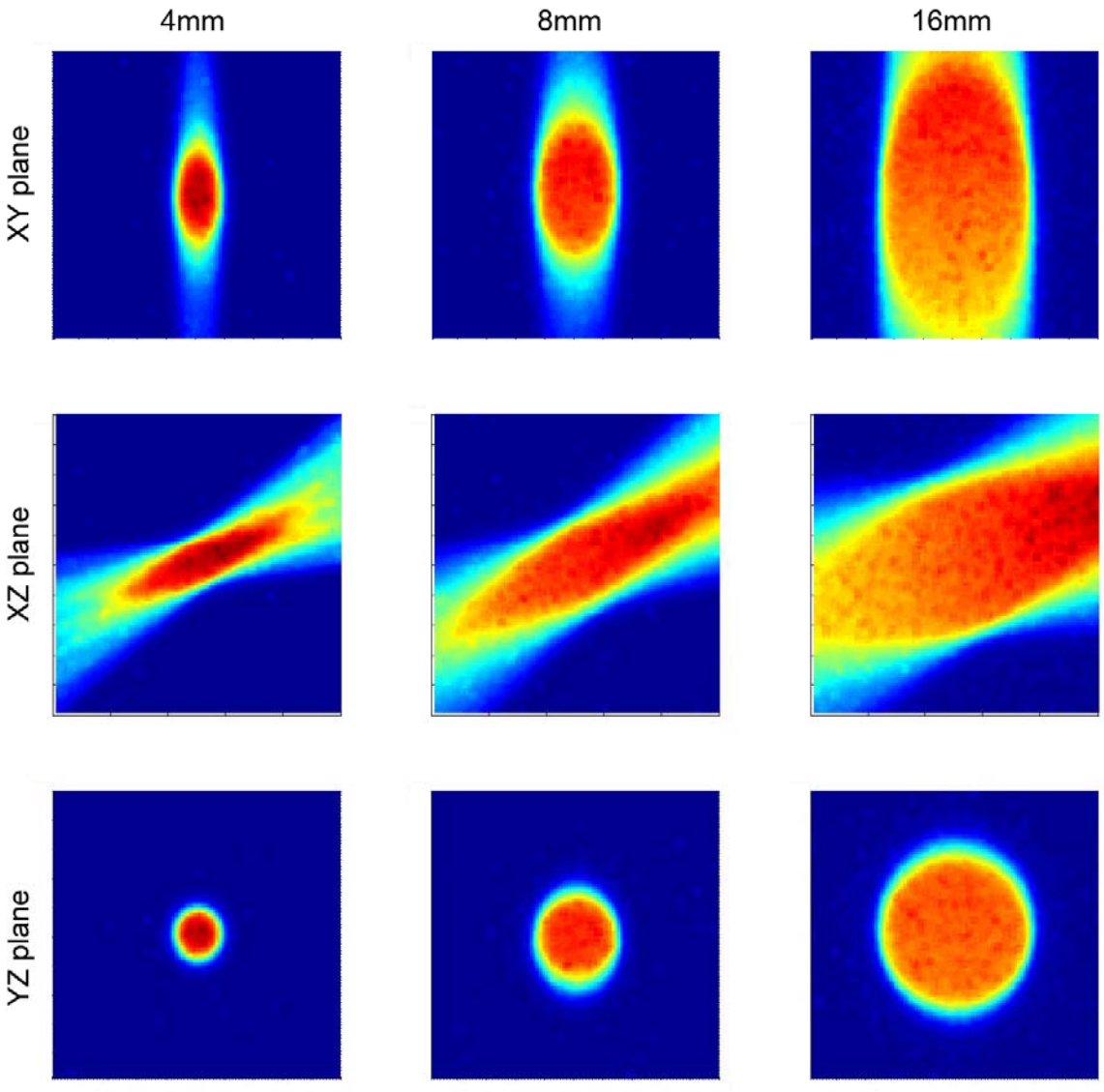

Figure 15: 3x3 cm dose distributions from all rows summed for each collimator, shown in each Cartesian plane. The data from the leftmost column of figure 14 (4 mm collimator data) were summed to produce the 4 mm collimator dose distribution in the leftmost column here, and so on for the other two collimators. Red areas are high dose, blue is low dose, on a linear scale normalized independently for each sub-image.

FWHM, profile curves, and rotated dose distributions

Another useful test of this simulation is the full width at half-max (FWHM) of each profile curve. The FWHM is the source of the collimators' names, since the 16 mm collimator's output is designed to have an approximate FWHM of 16 mm, and the same for 8 mm and 4 mm collimators. Our model placed one source per row, a very different setup from the Perfexion which has varying number of sources by row, and the beams arrive at angles off the XZ-plane seen in figures 14 and 15. But since the dosimetry sphere is symmetric about the z-axis, the individual source-row dose distribution can be rotated throughout its particular row to provide a simulation of the Perfexion with all 192 sources. An accurate measure of FWHM must take this three-dimensional aspect of the dose distributions into account.

The dose grid was manipulated with a program written in Matlab to rotate the three-dimensional dose distribution in steps about the z-axis and sum the individual, rotated dose distributions in order to simulate the total three-dimensional dose distribution delivered by the Perfexion. The dose distribution from each row was rotated independently in steps that matched the number of GK sources present in each row. For example: Row A has six sources per sector, so the row A dose distribution was rotated in 48 steps (6 sources/sector x 8 sectors) in increments of 7.5 degrees each to simulate the six sources in eight sectors. Row B has four sources per sector so its dose distribution was rotated over 32 steps in increments of 11.25 degrees each, and so on for the other rows. The dose distributions for the rotated rows were summed for each collimator. This dose distribution depends on the spherical symmetry of the 8 cm radius dosimetry sphere and is not accurate anywhere but near the center of the sphere where the beams converge.

Figure 7 shows that, unlike this stepwise rotation system, the actual GK sources are not uniformly spaced along their rows. Nonetheless, this equal-increment rotation provides a good dose distribution approximation near the center. These rotated dose distributions are shown in figure 16.

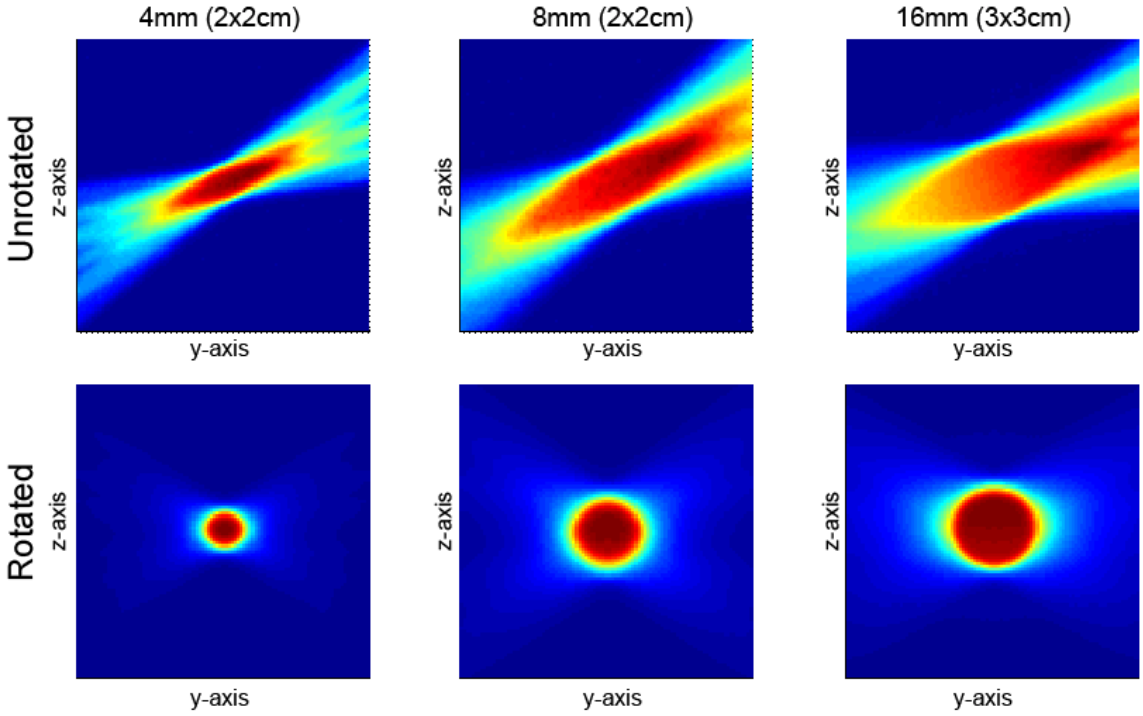

Figure 16: Dose distribution planes from each collimator after stepwise rotation of the dose distributions in figure 14 about the Z-axis in Matlab.

The dose along the center of the x- or y-axes of the artificially rotated dose distributions, along the centerlines of the images in figure 16, should mimic the dose profiles found across a shot from the Perfexion. These profiles are shown in figure 17.

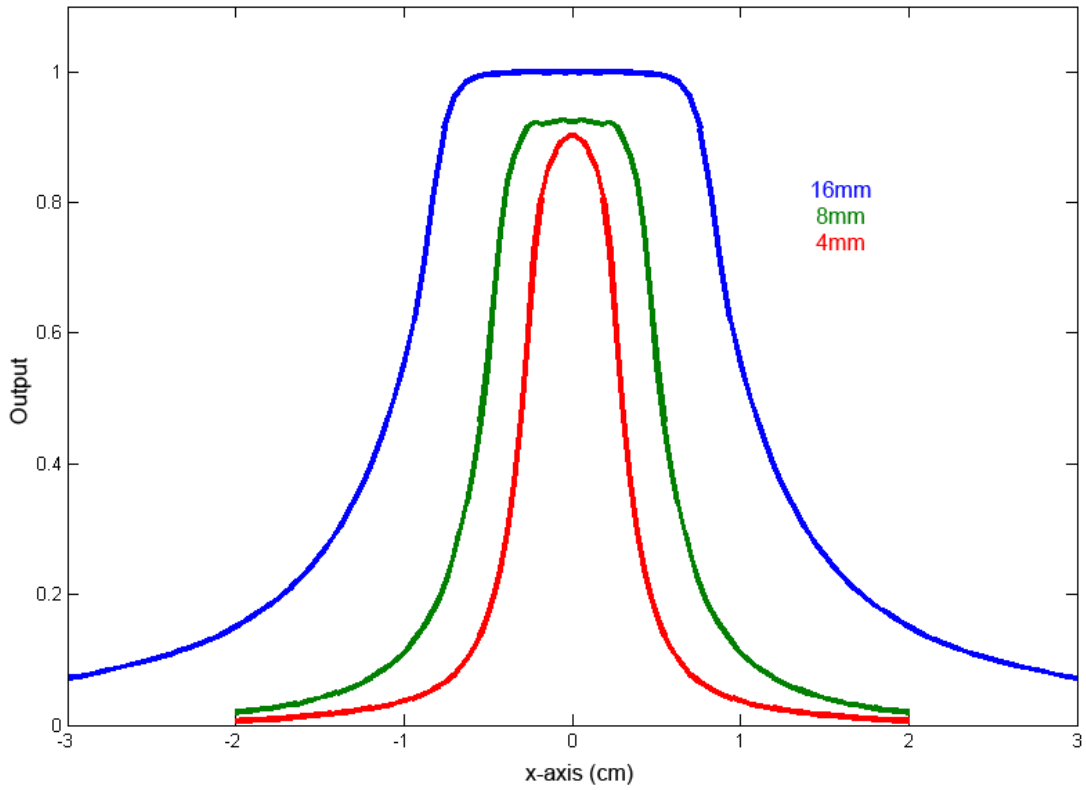

Figure 17: Dose profile curves produced by artificially rotating the single source dose distributions about the z-axis. These curves were used to calculate the FWHM of each collimator.

We evaluated the FWHM of the profiles shown in figure 17 and compared them to the manufacturer's values. Individual beams may nominally be 4, 8, or 16 mm, but the actual FWHM of the dose distribution based on all 192 sources is considerably wider, as shown in Table II. Our FWHM results were within 1 mm in all cases. The bin width for the profile curve was 0.4 mm.

Collimator	Measured (mm) ±0.4mm	Nominal Mfgr Value (mm)	Absolute, and % Difference
16 mm	20.4	21.3	-0.9mm, 4.2%
8 mm	11.2	10.8	0.4 mm, 3.7%
4 mm	6.4	6.0	0.4 mm, 6.7%

TABLE II: Full widths at half max for each collimator size from the profiles in figure 17.

The dose profile curves from figure 17 were individually compared to the film-based dose profile curves collected by Elekta at commissioning of the Perfexion. These curves are shown in figure 18-A through 18-C

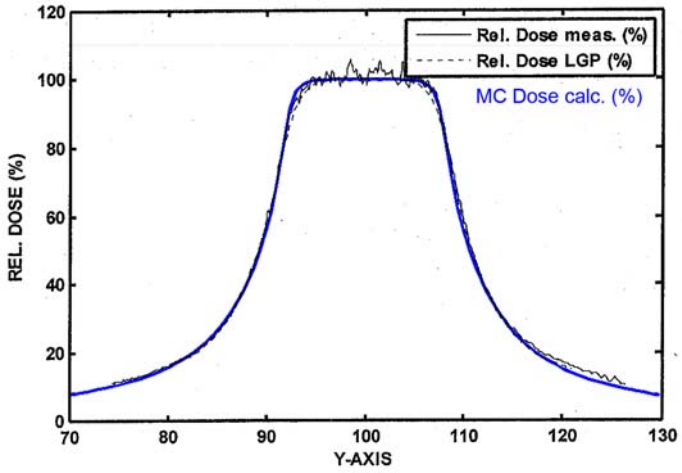

(**A**)

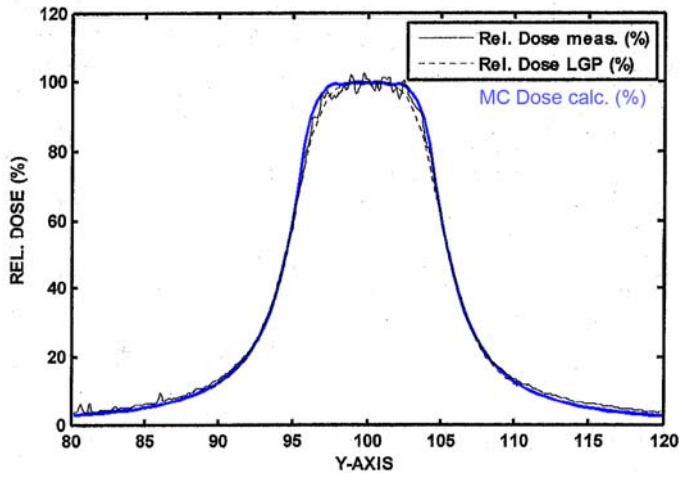

(B)

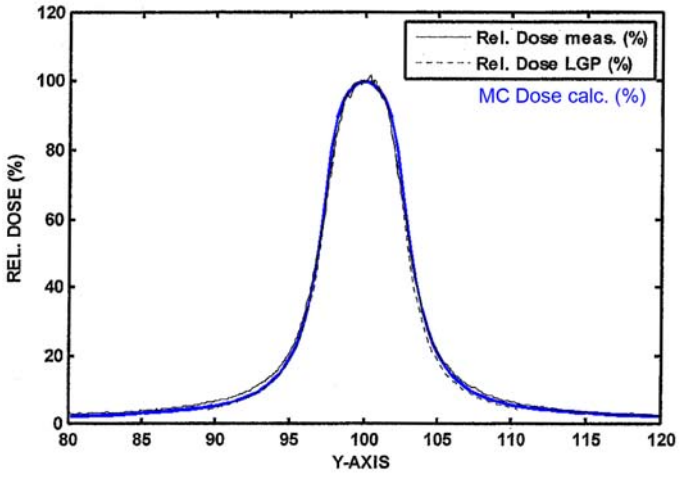

(C)

Figure 18: Dose profile curves calculated by MC in blue overlaid with film-based dose profile curves collected by an Elekta engineer at commissioning. (A) is the 16 mm collimator profile, (B) is the 8 mm profile, and (C) is the 4 mm profile.

The MC dose profile curves in figure 18 were overlaid by matching up the axes only. No other image manipulations were used.

Output Factors

Finally the row output factors and collimator output factors were calculated by recording the simulated dose deposited in a simple, mathematically defined dosimeter at the center of an 8 cm radius dosimetry sphere. The absolute doses were recorded for each row, and the row OFs were calculated by dividing each absolute dose by the dose from 16 mm collimator, row B. The row OF results are shown in table III and figure 19.

Collimator (mm)	Row	Elekta Row OF	Calculated Row OF	Row OF % difference	Elekta Collimator OF	Calculated Collimator OF	Collimator OF % diff.
16	A	0.961	**0.957**	-0.45%			
16	B	1.000	**1.000***	-			
16	C	0.986	**0.978**	-0.77%	1.000	**1.000***	-
16	D	0.920	**0.917**	-0.36%			
16	E	0.851	**0.851**	-0.05%			
8	A	0.957	**0.950**	-0.74%			
8	B	0.946	**0.948**	0.23%			
8	C	0.901	**0.890**	-1.20%	0.924	**0.922**	-0.24%
8	D	0.808	**0.803**	-0.57%			
8	E	0.730	**0.726**	-0.53%			
4	A	0.799	**0.777**	-2.70%			
4	B	0.815	**0.798**	-2.11%			
4	C	0.792	**0.781**	-1.36%	0.805	**0.792**	-1.55%
4	D	0.725	**0.713**	-1.66%			
4	E	0.663	**0.652**	-1.70%			

TABLE III: Output factors calculated through Monte Carlo simulation are compared to the reference values from the manufacturer, Elekta Instrument AB, Stockholm, Sweden.[38] Measured OFs are bolded, and the percent differences from the reference values are shown. All percent differences are under 3%. (* OFs for the 16 mm collimator and row B – 16 mm collimator are the base, relative values and defined as unity)

Table III also shows the collimator output factors, which were calculated by weighted sum across the doses from each collimator's rows, and dividing by the 16 mm collimator's absolute dose. The calculated output factors were well within 1% of Elekta's 8 mm collimator OF, and within 2% of Elekta's 4 mm collimator OF.

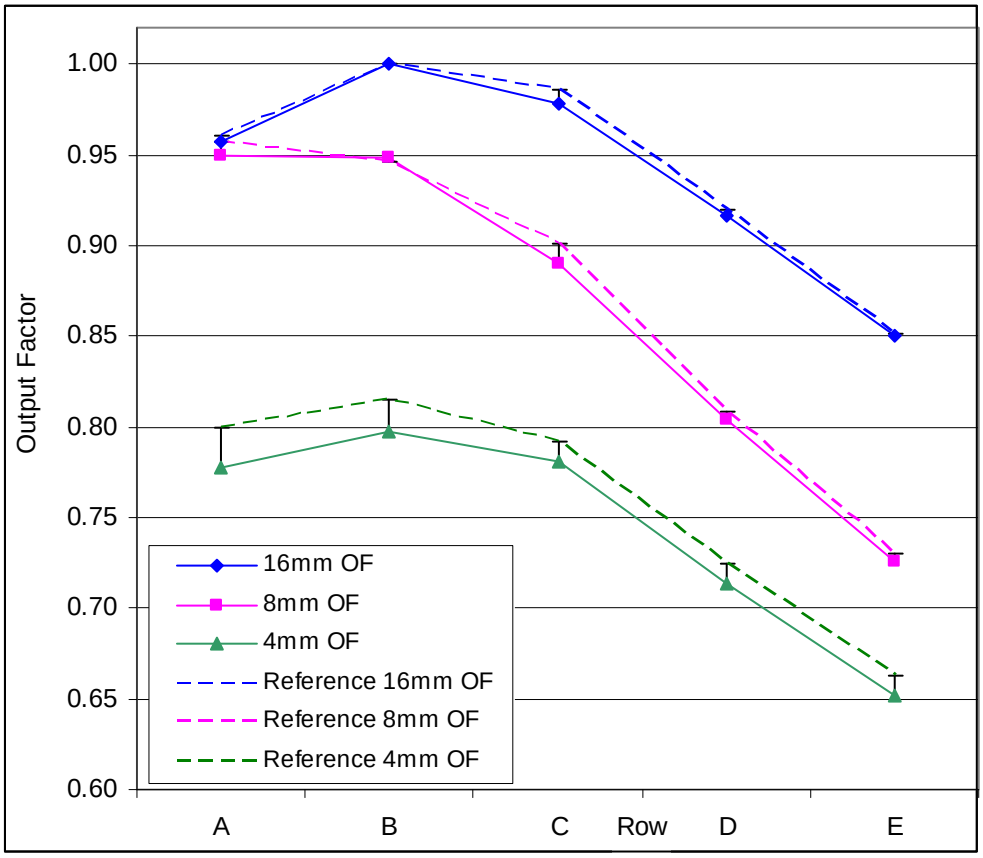

Figure 19: Calculated row output factors (solid lines) and the reference values from Elekta AB (dashed lines).

These output factors were measured over a dose computation volume 3.3 mm in diameter, a size that is about one-half the size of the Capintec PR-05P ion chamber[53] used by our facility for dose constancy measurements. We found the 4 mm OFs strongly depended on the volume over which they were measured due to the lack of a flat plateau at the peak dose region of the 4 mm collimator's output. Figure 20 shows the strong dependence of the 4 mm output factor on the area over which it is calculated.

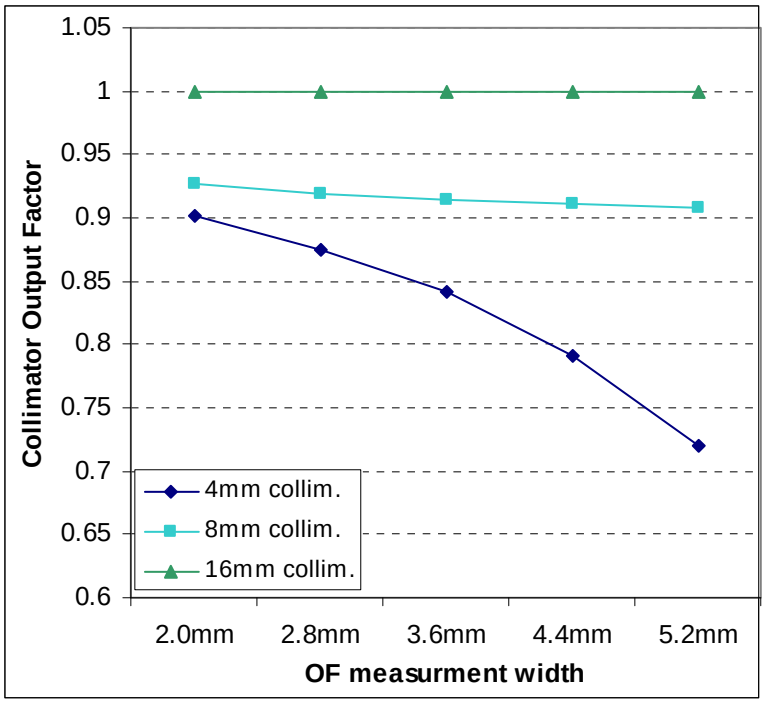

Figure 20: Some collimator OFs depend strongly on their area of measurement. The 8 mm collimator OF is relatively stable over a range of measurement volumes, but the 4 mm collimator OF is highly dependent on measurement method.

DISCUSSION

The dose distributions shown in figures 14 and 15 show that the MC simulation is qualitatively accurate. The beams are intersecting and entering the volumes from the angles expected and show attenuation that increases with depth, as predicted. The spectra collected make sense for a Cobalt-60 source delivering the energy spectrum to a volume of simulated water. The FWHM measurements generated by rotating the dose distributions are accurate to within 1 mm for all collimators. There is strong agreement between the MC dose profile curves and the film-based curves from commissioning. The row output factors measured by our Penelope simulations are in all cases less than 3% different from the reference values provided by Elekta which are used for dosimetry

calculations and treatment planning. The collimator output factors we calculated were within 2% of the manufacturer's values in both cases. These accuracies demonstrate the Penelope Monte Carlo code created is a good model of the GK Perfexion for all rows and collimators delivering doses near the isocenter in an idealized geometry.

One important problem with this work, along with other papers which give output factors, is the nonstandard size of the defined central plateau where the OF was measured. Others have found the Perfexion collimator OFs in agreement of the Elekta reference numbers, but have not defined the area over which the OF was measured.[38,47,48] These OF measurements were made using film dosimetry which, as an experimental measure, leaves some uncertainty as to the area over which the measurement is taken. Ideally the OF is measured at an infinitesimal point in the center (peak) of the dose distribution, but experimentally the measurement must take place over a finite area. Figure 21 shows the finite area over which this study measured the output factors – a diameter of 3.3mm. The 16 mm and 8 mm profiles are flat plateaus in this region, but the 4 mm profile is significantly curved. Our measurements' agreement with the manufacturer's output factors is made possible in part by a judicious choice of detector volume.

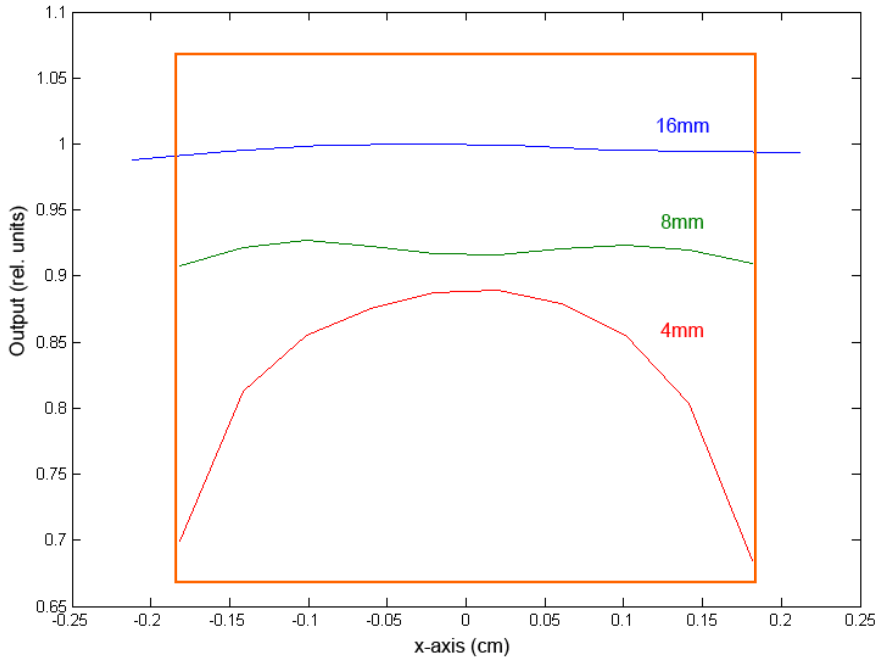

Figure 21: Output factors were measured over the boxed portions of the dose profiles. The 4 mm profile curve is not as flat as would be ideal.

There are two possible causes for the non-flat 4 mm profile matching the OF provided by the manufacturer and other publications.[38,47,48] First, our model either overestimates the dose delivered by the central, flat plateau of the 4 mm collimator by approximately 7%, or underestimates the dose delivered by the 18 mm collimator (since the OF is a ratio of the absolute outputs for the 4 mm and 16 mm collimators). Second, previous publications integrated over a similar area when calculating their output factors, and/or did not know or disclose the region measured. Figure 20 shows the strong dependence of the 4 mm collimator's OF on the area over which it is calculated, which is as expected due to the very small field size and is consistent with other publications (e.g., Reference 2). This research chose a reference volume equivalent to a small-volume ionization chamber that resulted in a match for published and experimental values. Clearly, definition of the measurement volume is important for small field modeling. Future work by this author

will address this measurement volume discrepancy by modeling radiation detectors, such as ionization chambers, directly in the simulation, thereby bypassing problems associated with air-filled dosimeters approximated as uniform spheres.

CONCLUSIONS

The scope of this project was to 1) create a working MC simulation using Penelope; 2) define the geometry of Perfexion within the Penelope language; and 3) calculate output factors, including an initial study of the volume dependence of those output factors. The Penelope code is up and running using the parallel architecture of the DEAC cluster. The simulation uses Perfexion's geometry provided by the manufacturer written in the Penelope geometry language PENGEOM. Output factor measurements represent a proof of concept on the implementation of these tools. The three objectives were accomplished, and represent a status report on this research project.

Future work will complete modeling the Perfexion by modeling each of the 24 sources per sector for each collimator size. Dose distributions will be recorded near the isocenter as well as distant from the center in order to verify simulation accuracy. Radiochromic film and gel measurements on the GK Perfexion will be compared with MC-calculated Penelope dose distributions for a variety of clinically and research relevant irradiation geometries. The variations in FWHM measurements, and the possible influence of cutoff energies, will be investigated. With phase space files recording the output of a full sector it will be possible to deliver that fluence to any simulated target and compare the results directly to experimental results on the Perfexion. In particular, once the MC simulation is experimentally validated, this simulation tool will allow researchers to simulate dose

distributions in research scenarios without being limited by the proprietary manufacturer's simulation algorithm.

REFERENCES

1. Attix, F.H. *Introduction to Radiological Physics and Radiation Dosimetry*, (John Wiley & Sons, New York, 1986).

2. Das, I., J., George, X.D. & Anders, A. Small fields: Nonequilibrium radiation dosimetry. *Medical Physics* **35**, 206-215 (2008).

3. Khan, F.M. *The Physics of Radiation Therapy*, (Lippincott Williams & Wilkins, Philadelphia, PA, 2003).

4. Task Group 21, R.T.C., American Ass'n of Physicists in Medicine. A protocol for the determination of absorbed dose from high-energy photon and electron beams. *Medical Physics* **10**, 741-771 (1983).

5. Almond, P.R. et al. AAPM's TG-51 protocol for clinical reference dosimetry of high-energy photon and electron beams. *Medical Physics* **26**, 1847-1870 (1999).

6. Li, X.A., Soubra, M., Szanto, J. & Gerig, L.H. Lateral electron equilibrium and electron contamination in measurements of head-scatter factors using miniphantoms and brass caps. *Medical Physics* **22**, 1167-1170 (1995).

7. Turner, J.E. *Atoms, Radiation, and Radiation Protection*, (John Wiley & Sons, Inc., New York, 1995).

8. Salvat F, F.-V.J.M.a.S.J. *PENELOPE - A Code System for Monte Carlo Simulation of Electron and Photon Transport*, (NEA-OECD, Paris, 2003).

9. Sauter, F. Über den atomaren Photoeffekt in der K-Schale nach der relativistischen Wellenmechanik Diracs. *Ann. Phys.* **11**, 454-488 (1931).

10. Knoll, G.F. *Radiation Detection and Measurement*, (Wiley & Sons, Ann Arbor, MI, 2000).

11. Sauer, O.A. & Wilbert, J. Measurement of output factors for small photon beams. *Medical Physics* **34**, 1983-1988 (2007).

12. Seuntjens, J. & Verhaegen, F. Comments on 'Ionization chamber dosimetry of small photon fields: A Monte Carlo study on stopping-power ratios for radiosurgery and IMRT beams'". *Physics of Medicine and Biology* **48**, L43-45 (2003).

13. Kijewski, P.K., Bjangard, B.E. & Petti, P.L. Monte Carlo calculations of scatter dose for small field sizes in a 60C beam. *Medical Physics* **13**, p74-77 (1986).

14. Ding, G.X., Duggan, D.M. & Coffey, C.W. Commissioning stereotactic radiosurgery beams using both experimental and theoretical methods. *Phys Med Biol* **51**, p2549-2566 (2006).

15. Ding, G.X. Dose discrepancies between Monte Carlo calculations and measurements in the buildup region for a high-energy photon beam. *Medical Physics* **29**, p2459-2463 (2002).

16. Paelinck, L., Reynaert, N., Thierens, H., Neve, W.D. & Wagtner, C.D. Experimental verification of lung dose with radiochromic film: Comparison with Monte Carlo simulations and commercially available treatment planning systems. *Phys Med Biol* **50**, p2055-2069 (2005).

17. Kahn, H. Random sampling (Monte Carlo) techniques in neutron attenuation problems--I. *Nucleonics* **6**, 27 (1950).

18. Rogers, D.W. Fifty years of Monte Carlo simulations for medical physics. *Phys Med Biol* **51**, R287-301 (2006).

19. Andreo, P. Monte Carlo techniques in medical radiation physics. *Phys Med Biol* **36**, 861-920 (1991).

20. Berger, M.J., Wang, R. Multiple-scattering angular deflections and energy-loss straggling. in *Monte Carlo Transport of Electrons and Photons* (ed. T M Jenkins, W.R.N., A Rindi) p21-56 (Plenum, New York, 1988).

21. Berger, M.J., Wang, R. Monte Carlo calculation of the penetration and diffusion of fast charged particles. *Methods in Computational Physics* **v1**(1963).

22. Baro J, S.J., Fernandez-Varea J M, Salvat F. PENELOPE: An algorithm for Monte Carlo simulation of the penetration and energy loss of electrons and positrons in matter. *Nuclear Instruments and Methods in Physics Research B* **100**, p31-46 (1995).

23. DesRosiers, C., Moskvin, V., Bielajew, A.F. & Papiez, L. 150-250 meV electron beams in radiation therapy. *Phys Med Biol* **45**, 1781-805 (2000).

24. Sempau, J. et al. Monte Carlo simulation of electron beams from an accelerator head using PENELOPE. *Phys Med Biol* **46**, 1163-86 (2001).

25. Moskvin, V. et al. Monte Carlo simulation of the Leksell Gamma Knife: I. Source modelling and calculations in homogeneous media. *Phys Med Biol* **47**, 1995-2011 (2002).

26. Papiez, L., DesRosiers, C. & Moskvin, V. Very high energy electrons (50-250 MeV) and radiation therapy. *Technol Cancer Res Treat* **1**, 105-10 (2002).

27. DesRosiers, P.M. et al. Lung cancer radiation therapy: Monte Carlo investigation of "under dose" by high energy photons. *Technol Cancer Res Treat* **3**, 289-94 (2004).

28. Moskvin, V. et al. Monte Carlo simulation of the Leksell Gamma Knife: II. Effects of heterogeneous versus homogeneous media for stereotactic radiosurgery. *Phys Med Biol* **49**, 4879-95 (2004).

29. Al-Dweri, F.M.O., Rojas, E.L. & Lallena, A.M. Effects of bone- and air-tissue inhomogeneities on the dose distributions of the Leskell Gamma Knife(R) calculated with PENELOPE. *Phys Med Biol* **50**, p5665-5678 (2005).

30. Das I.J., K.A., Verhaegen F, Moskvin, V.P. Interface Dosimetry: measurements and Monte Carlo simulations of low-energy photon beams. *Radiation Physics and Chemistry* **61**, p593-595 (2001).

31. Das I.J., M., V.P., Kassaee A, Tabata T, Verhaegen F. Dose perturbations at high-Z interfaces in kilovoltage photon beams: comparison with Monte Carlo simulations and measurements. *Radiation Physics and Chemistry* **64**, p173-179 (2002).

32. Cheung, J.Y. & Yu, K.N. Rotating and static sources for gamma knife radiosurgery systems: Monte Carlo studies. *Med Phys* **33**, 2500-5 (2006).

33. Novotny Jr J, B.J., Niranjan A, Quader MA, Saiful Huq M, Bednarz G, Flickinger J, Kondziolka D, Lunsford LD. Dosimetric comparison of the Leksell Gamma Knife Perfexion and 4C. *Journal of Neurosurgery* **109**, p8-14 (2008).

34. Lundquist C, P.I. The Leksell Gamma Knife Perfexion and comparisons with its predecessors. *Operative Neurosurgery* **61**, p130-141 (2007).

35. Wiant, D. et al. Gamma knife radiosurgery treatment planning for small animals using high-resolution 7T micro-magnetic resonance imaging. *Radiat Res* **172**, 625-31 (2009).

36. Cheung, J.Y., Yu, K.N., Ho, R.T. & Yu, C.P. Monte Carlo calculated output factors of a Leksell Gamma Knife unit. *Phys Med Biol* **44**, N247-9 (1999).

37. Leskell Gamma Plan 8.2 Online Reference Manual. Rev.01 edn (ELEKTA Instruments AB, Stockholm, Sweden, 2007).

38. Novotny, J., Jr. et al. Measurement of relative output factors for the 8 and 4 mm collimators of Leksell Gamma Knife Perfexion by film dosimetry. *Med Phys* **36**, 1768-74 (2009).

39. Bednarz, G., Huq, M.S. & Rosenow, U. Deconvolution of dtector size effect for output factor measurement for narrow Gamma Knife radiosurgery beams. *Phys Med Biol* **47**, 3643-3649 (2002).

40. Mack, A. et al. Precision dosimetry for narrow photon beams used in radiosurgery-determination of Gamma Knife output factors. *Med Phys* **29**, 2080-9 (2002).

41. Tsai, J.S. et al. Determination of the 4 mm Gamma Knife helmet relative output factor using a variety of detectors. *Med Phys* **30**, 986-92 (2003).

42. Araki, F., Ikegami, T., Ishidoya, T. & Kubo, H.D. Measurements of Gamma-Knife helmet output factors using a radiophotoluminescent glass rod dosimeter and a diode detector. *Med Phys* **30**, 1976-81 (2003).

43. Ekstrand, K.E. & Bourland, J.D. A film technique for the determination of output factors and end effect times for the Leksell Gamma Knife. *Phys Med Biol* **46**, 703-6 (2001).

44. Kurjewicz, L. & Berndt, A. Measurement of Gamma Knife helmet factors using MOSFETs. *Med Phys* **34**, 1007-12 (2007).

45. Gasparian, P.B.R. et al. Demonstrating the use of optically stimulated luminescence dosimeters (OSLDs) for measurement of staff radiation exposure in interventional fluoroscopy and helmet output factors in radiosurgery. *Radiation Measurements* **45**, 677-680.

46. Moutsatsos, A. et al. Gamma knife output factor measurements using VIP polymer gel dosimetry. *Med Phys* **36**, 4277-87 (2009).

47. Ma, L. et al. A simple and effective method for validation and measurement of collimator output factors for Leksell Gamma Knife Perfexion. *Phys Med Biol* **54**, 3897-907 (2009).

48. Bhatnagar, J.P. et al. First year experience with newly developed Leksell Gamma Knife Perfexion. *J Med Phys* **34**, 141-148 (2009).

49. Trnka, J., Novotny, J., Jr. & Kluson, J. MCNP-based computational model for the Leksell gamma knife. *Med Phys* **34**, 63-75 (2007).

50. Kjäll, P. & Johansson, J. Geometry information for Gamma Knife Perfexion. (ed. Best, R.) 11 (Elekta Instrument AB, Stockholm, 2010).

51. Elekta, A.B. Safety Evaluation of Sealed Source - Medical Teletherapy Source. 10 (Elekta A.B., 2007).

52. Salvat F, F.-V.J.M.a.S.J. *PENELOPE - A Code System for Monte Carlo Simulation of Electron and Photon Transport*, (NEA-OECD, Paris, 2008).

53. Capintec, I. Capintec, Inc. product information brochure. (Capintec, Inc., 2003).

54. Bielajew, A.F., Rogers, D. W. O. Variance Reduction techniques. in *Monte Carlo transport of Electrons and Photons* (ed. Jenkins, T.M.) (Plenum, New York, 1988).

55. Miller, T., David Chin. Information for Grant Writing. in *WFU DEAC Support Wiki* Vol. 2010 (Wake Forest University, Winston-Salem, NC, 2010).

VITA

Ryan Best is from Ashland, near Richmond, Virginia. He did his undergraduate work at Guilford College in Greensboro, NC, and in 2003 received Bachelor of Science degrees in Physics with honors, and Computing & Information Technology. While at Guilford College he received the Jeglinski Physics Award and membership in Sigma Pi Sigma, the physics honors society. After college he worked for Gamma Corporation, a Medical/Health Physics consulting company in Honolulu, Hawaii. During that time he took graduate courses in Medical Physics from Georgia Tech in Atlanta, Georgia through a distance learning program. In 2006 he returned to graduate study at Wake Forest University in Winston-Salem, NC where he is supported by a clinical assistantship at the Department of Radiation Oncology at Wake Forest University Baptist Medical Center. His research is published in the Journal of Applied Clinical Medical Physics[1] (JACMP) and the Journal of Computer Assisted Tomography[2] (JCAT), and was presented at the conferences of the American Association of Physicists in Medicine (AAPM) in 2009 and 2010, and American Society for Radiation Oncology (ASTRO) in 2010. He plans to continue this research as part of a doctoral dissertation.

Vita References

1. Gersh, J.A. et al. Improved volumetric imaging in tomosynthesis using combined multiaxial sweeps. *Journal of Applied Clinical Medical Physics* **11**(2010).

2. Bharkhada, D. et al. Demonstration of Dose and Scatter Reductions for Interior Computed Tomography. *J. of Computer Assisted Tomography* **33**, 967-972 (2009).